EVALUATION OF CHARGING AND DISCHARGING PERFORMANCES OF THE RECHARGEABLE ALUMINIUM-AIR BATTERY

KHOO WEN LOONG

UNIVERSITI TUNKU ABDUL RAHMAN

EVALUATION OF CHARGING AND DISCHARGING PERFORMANCES OF THE RECHARGEABLE ALUMINIUM-AIR BATTERY

KHOO WEN LOONG

A project report submitted in partial fulfilment of the requirements for the award of Bachelor of Engineering (Honours) Mechanical Engineering

Lee Kong Chian Faculty of Engineering and Science
Universiti Tunku Abdul Rahman

September 2022

DECLARATION

I hereby declare that this project report is based on my original work except for citations and quotations which have been duly acknowledged. I also declare that it has not been previously and concurrently submitted for any other degree or award at UTAR or other institutions.

Signature   :

Name   :   Khoo Wen Loong

ID No.   :   1800218

Date   :   2th October 2022

APPROVAL FOR SUBMISSION

I certify that this project report entitled **"Evaluation of Charging and Discharging Performances of the Rechargeble Aluminium-Air Battery"** was prepared by **Khoo Wen Loong** has met the required standard for submission in partial fulfilment of the requirements for the award of Bachelor of Engineering (Honours) Mechanical Engineering at Universiti Tunku Abdul Rahman.

Approved by,

Signature	:	*bernard saw*
Supervisor	:	Dr. BERNARD SAW LIP HUAT
Date	:	3/10/2022

Signature	:	
Co-Supervisor	:	
Date	:	

The copyright of this report belongs to the author under the terms of the copyright Act 1987 as qualified by Intellectual Property Policy of Universiti Tunku Abdul Rahman. Due acknowledgement shall always be made of the use of any material contained in, or derived from, this report.

ACKNOWLEDGEMENTS

I would like to thank everyone who had contributed to the successful completion of this project. I would like to express my gratitude to my research supervisor, Dr. Bernard Saw Lip Huat for his invaluable advice, guidance and his enormous patience throughout the development of the research.

In addition, I would also like to express my gratitude to my Mr. Tan Wen Cheong for his support and assistance on the lab apparatus and equipments.

ABSTRACT

Batteries are essential energy storage system widely utilized in our daily lives. Batteries provide power to the portable devices in our daily lives including car keys, laptops, smartphones, and vehicles. There are many types of batteries, the examples of these batteries include lithium-ion battery, alkaline battery, and metal-air battery. Recently, since the commercial lithium-ion battery is approaching its performance limit, the development of electric vehicles has encouraged the research on metal-air batteries, including the aluminium-air battery. High theoretical energy density of aluminium-air battery and the lightweight, wide availability at low cost, and safety of aluminium has further motivated the research in aluminium-air battery. In this project, a rechargeable aluminium-air battery was designed and developed using economic materials such as carbons, acrylics, and kitchen aluminium foil. This project consists of several findings. First of all, the mesh type current collector with greater number of openings per meter square provides better battery performance. Next, the optimum loadings of reduced graphene oxide are 15 mg in total of 330 mg of catalyst mixture (approximately 4.5% mass ratio). For separators, non-woven membrane (glass fiber separator) allows better battery performance than cellulose membrane (filter paper separator). With the combinations of the components that provides the best results, the developed aluminium-air battery was able to exhibits the energy density of 297 mWh/g. Finally, addition of additives into the aqueous electrolyte was able to inhibits the formation for aluminium hydroxide and parasitic hydrogen evolution reaction. However, the suppression of the impurities and the hydrogen evolution does not provide the battery with long-term rechargeability.

TABLE OF CONTENTS

LIST OF TABLES

LIST OF FIGURES

LIST OF SYMBOLS / ABBREVIATIONS

c_p	specific heat capacity, J/(kg·K)
h	height, m
K_d	discharge coefficient
M	mass flow rate, kg/s
P	pressure, kPa
P_b	back pressure, kPa
R	mass flow rate ratio
T	temperature, K
v	specific volume, m^3
α	homogeneous void fraction
η	pressure ratio
ρ	density, kg/m^3
ω	compressible flow parameter
ID	inner diameter, m
MAP	maximum allowable pressure, kPa
MAWP	maximum allowable working pressure, kPa
OD	outer diameter, m
RV	relief valve

CHAPTER 1

INTRODUCTION

1.1   General Introduction

Batteries are essential chemical energy storage widely utilized in our daily lives. The application of batteries in our daily lives includes clocks, remote controls, electronic keys, laptops, smartphones, and vehicles. Batteries provide electricity to portable devices by converting chemical energy to electrical energy. According to Parlemo (2015), a battery consists of three main components: anode, cathode, and electrolyte. These three components produce electricity by creating the flow of electrons through an electrochemical reaction is known as the oxidation-reduction (redox) reaction. During the redox reaction, oxidation reaction at anode produces electrons. Next, the electrons will flow through an external connection to the cathode for the reduction reaction. The flow of electrons induces a current that flows in the opposite direction (Woodford, 2021). This current is the electricity that provides power to the portable devices in our daily lives.

There are many different types of batteries with different shapes and sizes designed for various applications. According to Woodford (2021), there are also two categories to differentiate these batteries: the non-rechargeable batteries (also known as primary batteries) and the rechargeable batteries (also known as secondary batteries). Examples of primary batteries include zinc-carbon batteries, alkaline batteries, and silver-oxide batteries. The zinc-carbon and alkaline batteries are the most common single-use cylindrical-shaped batteries used in cameras, remote controls, and clocks. As for silver-oxide batteries, they are small-sized button-shaped batteries used in watches and electronic keys. Next, examples of secondary batteries include lithium-ion batteries, nickel-cadmium (NiCd) batteries, and metal-air batteries. These batteries come in different shapes based on the application. The application of these rechargeable batteries includes laptops and motor vehicles. The main difference between batteries of these two categories is that the chemical reaction is irreversible in non-rechargeable batteries while reversible in rechargeable batteries.

The rechargeable batteries provide electricity by converting chemical energy to electrical energy like any commercial battery. These batteries are rechargeable due to the anode, cathode, and electrolyte used. The charging mechanism for a rechargeable battery is by using the concept of electrolytic cells. Electrolytic cells drive the oxidation reaction on the cathode and reduction reaction on the anode by using an external power source. The external power source creates a movement of electrons from the anode to the cathode and enables the redox reaction. Among rechargeable batteries, metal-air batteries with higher theoretical energy density than lithium-ion batteries are promoted frequently as a solution toward next-generation electrochemical energy storage for electric vehicles and other applications (Li & Lu, 2017). The theoretical energy density of the battery is the amount of energy stored in the battery per unit mass. Given the battery with the same mass and size, the higher the theoretical energy density, the higher the energy stored within the battery. Furthermore, lithium-ion battery technology is approaching its performance limit, and it is difficult for conventional lithium-ion battery-powered electrical vehicles (EVs) to achieve long driving ranges (Li & Lu, 2017).

Among metal-air batteries, aluminium-air battery (AAB) is attractive due to its aluminium anode lightweight, wide availability at a lost cost, and safety (Buckingham, et al., 2021). Like all the batteries, AAB uses high purity aluminium as the anode, an air cathode that reduces oxygen from the surrounding air, and alkaline such as potassium hydroxide (KOH) or sodium hydroxide (NaOH) as the electrolyte (Tang, et al., 2018). The air cathode of an AAB battery is composed of a current collector, a gas diffusion layer, and a catalyst to drive the oxygen reduction reaction (ORR) (Mori, 2020). According to Mori (2020), the current collector of the air cathode functions to connect to external electrical circuits and transfer electrons and electricity. For the gas diffusion layer, the function is to absorb air from the surrounding air and seal the battery to prevent the leakage of liquid electrolytes (Mori, 2020). Apart from the three main components of batteries, a separator also is a critical battery component. The function of a battery separator is to isolate the anode and cathode to prevent short circuit issues while allowing the ions to cross through the battery separator (Tan, et al., 2021).

1.2   Importance of the Study

According to Arroyo and Miguel (2019), the transportation sector has represented more than 50% of the energy consumption matrix. It has been identified as the most inefficient sector in energy consumption due to the use of hydrocarbons (fossil fuel and petroleum) in large measures (Arroyo & Miguel, 2019). Furthermore, the high usage of fossil fuels contributed to the emission of greenhouse gas and caused climate changes (Day & Day, 2017). Thus, policies to slow down fossil fuels extraction and the consumption of fossil fuels have gained attention globally. As the countermeasures to reduce fossil fuel usage and tackle climate change, electrical vehicles (EVs) using electrical motors to replace combustion engines have become the focus of researchers. The development of EVs has further encouraged research on metal-air batteries, including the AAB.

In summary, this research may contribute to the development of EVs and ultimately protect the environment by reducing the consumption of fossil fuels and the release of greenhouse gases. This research also can contribute to the achievement of Sustainable Development Goal 7 (affordable and clean energy) as the AAB does not generates energy with sources that releases pollutants. Finally, this research may provide a better understanding of how to evaluate the charging and discharging performance of an AAB.

1.3   Problem Statement

Despite all the advantages aluminium-air battery provides, there are also some drawbacks in the current design of the aluminium-air battery. Firstly, a parasitic chemical reaction called hydrogen evolution will occur on the pure aluminium anode and release hydrogen (Ju, et al., 2021). This chemical reaction will ultimately cause the failure of the aluminium-air battery (Liu, et al., 2017). After that, the battery separators are an essential component for compact and small batteries. These separators functions to prevent any physical contact between the anode and cathode of the battery (Zhang, 2007). Currently, there are only a few research on the battery separator for AAB. Furthermore, the effect of the separator in the rechargeable AAB are also unclear.

1.4   Aim and Objectives

The main aim of this study is to evaluate the charging and discharging performance of an aluminium-air battery. The three specific objectives to achieve the purpose of this research are as below:

   i.   Design and develop a rechargeable aluminium-air battery.

  ii.   To investigate the effect of different separators on the performance of the aluminium-air battery.

 iii.   To characterize the charging and discharging characteristics of the aluminium-air battery.

1.5   Scope and Limitation of the Study

For the scope of this study, a rechargeable AAB was developed using kitchen aluminium foil, potassium hydroxide electrolyte with ethyl-acetate additive, air cathode fabricated using reduced graphene oxide, activated carbon, and carbon black, and commercially available filter membranes as battery separator. The filter membrane used in this study are glass fiber filter membrane and normal laboratory filter paper (cellulose-based filter).

Next, the limitation of this study is first of all, the ionic liquids electrolyte was unable to obtain due to the insufficient budget and the materials to prepare the ILs not available in the university. Finally, there is only two separators used in this study. The number of data to compare the effect of separators are insufficient.

1.6   Contribution of the Study

This study has demonstrated the design and fabrication process of an AAB. The materials and the fabrication process of the most complicated component of the AAB, the air cathode are also demonstrated in this study. After that, this study can provide the feasibility of aqueous electrolyte for the rechargeable AAB. This study can also demonstrate the optimum loadings of reduced graphene oxide, which act as the catalyst to improve the oxygen reduction reaction. Finally, this study will also provide the effect of the separator surface on the performance of the AAB.

1.7   Outline of the Report

In this report, the first section shows the brief introduction of the AAB, importance of the study, problem statement, aims and objectives, scope and limitation of the study, and contribution of the study. After that, the second chapter shows the literature and journal articles that are being reviewed. The articles regarding the research done onto the anode, cathode, electrolyte, and separator of the AAB are also included. Thirdly, chapter three shows the methodology and work plan of this study. Chapter three includes the flowchart of the project, materials used in the project, component fabrication method, and battery assembly method are described in this chapter. The Gantt chart showing the project deadlines and milestones is also included in this chapter. Finally, chapter four shows the results and discussions of the project while chapter five shows the conclusion of the entire project.

CHAPTER 2

LITERATURE REVIEW

2.1 Introduction

This chapter highlights the investigation done in the development and commercialization of AABs. The novels regarding the research done on each essential component (anode, cathode, and electrolyte) are reviewed and described in this chapter. After that, literature regarding battery separators is also reviewed and discussed in this chapter. Notably, the literature reviewed here includes both primary and secondary AABs. There are also novels discussed in this chapter that is not conducted based on AABs. The literature regarding experiments conducted using different metal-air batteries, such as zinc-air batteries, is being reviewed and discussed in this chapter is to provide an innovative approach and show the inadequacies in the previous studies regarding AABs.

2.2 Aluminium-Air Battery

According to Li and Lu (2017), metal-air batteries have higher theoretical energy densities than lithium-ion batteries. The lithium-air battery has the highest theoretical specific energy among other metal-air batteries with 5210 $Whkg^{-1}$ including oxygen and 11140 $Whkg^{-1}$ excluding oxygen (Li & Lu, 2017). Although having the highest theoretical specific energy among other metal-air batteries, the lithium-air battery is difficult to obtain due to the instability of the lithium in a humid environment that necessitates the hermetical sealing effect (Mori, 2020). On the other hand, although having the second-highest theoretical specific energy among other metal-air batteries with a total of 4300 $Whkg^{-1}$ including oxygen and 8140 $Whkg^{-1}$ excluding oxygen, the lightweight, wide availability at a lost cost, and safety features of the aluminium anode of AAB make the AAB attractive (Buckingham, et al., 2021). These attractive features of the aluminium anode of AAB have made the AAB becomes a topic to research and further study.

2.2.1 Anode

Several studies were conducted on the aluminium anode material to achieve an optimum solution for the anode design. For pure aluminium anodes, Cho, et al. (2015) have experimented with 2N5 commercial grade aluminium with 99.5% purity and 4N high pure grade aluminium with 99.99% purity to study the influence of aluminium purity on the performance of AABs. The result shows that 2N5 grade Al has a lower battery performance than 4N grade Al at stand-by and low-power discharge. The 2N5 Al has lower battery performance is due to the formation of the complex film that mainly contains iron and silicon as impurities that impedes the ion exchange between the aluminium and electrolyte (Cho, et al., 2015). Although having higher aluminium purity allows higher battery performance, pure aluminium will undergo side reactions that discourage the electrochemical reactions and make the AAB unstable. According to Liu, et al. (2017), these side reactions include the formation of aluminium(III) oxide (Al_2O_3) and aluminium(III) hydroxide ($Al(OH)_3$) layer, formation of corrosion products such as aluminium(III) hydroxide ($Al(OH)_3$) and aluminate ion ($Al(OH)_3^-$)and parasitic corrosion reaction on the aluminium surface that produces hydrogen gas. Equation (2.1) below shows the parasitic corrosion reaction on the pure aluminium anode.

$$2Al + 6H_2O \rightarrow 2Al(OH)_3 + 3H_2 \qquad (2.1)$$
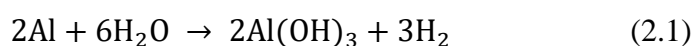
To overcome the parasitic corrosion issue, Hosseini, et al. (2022) suggest using acetoxy-group-based additives to protect the anode of AABs. The result shows that calcium acetate (Ca-Ac), barium acetate (Ba-Ac), and ethyl acetate in potassium hydroxide (KOH) electrolyte can inhibit the hydrogen evolution with inhibition efficiency of 34%, 50%, and 17%, respectively (Hosseini, et al., 2022). As for the effect of the additives on battery performance, the electrolyte without additives shows a maximum power density of 59.3 mWcm^{-2} at current densities of 65 mAcm^{-2} (Hosseini, et al., 2022). The maximum power density of the battery with calcium acetate, barium acetate, and ethyl acetate compared with potassium hydroxide electrolyte without additives experienced an increase of 24%, 50%, and 28%, respectively (Hosseini, et al., 2022). The result shows that the AABs with

electrolytes mixed with barium acetate and calcium acetate additives exhibit an approximately 22% higher discharge capacity than potassium hydroxide electrolytes without additives (Hosseini, et al., 2022).

Hosseini, et al. (2021) also used sulphur-oxygen (SO) group-based additives to reduce hydrogen evolution and improve the rechargeable AAB performance. The result shows that the addition of sodium sulphate (Na_2SO_4), sodium sulphite (Na_2SO_3), and dimethyl sulfoxide (C_2H_6SO) exhibits an increase in discharge capacities from 2021 mAhg^{-1} to 2604, 2393, and 2348 mAhg^{-1}, respectively (Hosseini, et al., 2021). The three additives also inhibit the hydrogen evolution rates with inhibition efficiency of 35%, 29%, and 42%, respectively (Hosseini, et al., 2021). From these two studies, the results show that both acetoxy-group-based and SO-group-based additives can inhibit the hydrogen evolution reaction (HER) and improve battery performance. These two studies also show that not all acetoxy-group-based and SO-group-based additives but only some specific additives are suitable for AABs. In other words, for acetoxy-group-based additives, barium acetate, calcium acetate, and ethyl acetate can inhibit the HER in AAB, as for SO-group-based additives, sodium sulphate, sodium sulphite, and dimethyl sulfoxide can inhibit the HER in AAB.

As for the solution to mitigate the self-corrosion of aluminium anode in alkaline electrolytes, Zhuang, et al. (2021) stated that doping aluminium anode materials with trace alloying elements may be an effective solution to attenuate self-corrosion and improve discharge performance. Zhuang, et al. (2021) have studied the influence of gallium element (Ga) on the electrochemical property and microstructure of the aluminium alloy as the anode for AABs. The result shows that Al alloy with Ga addition can lower mass-loss rate and higher discharge voltage than Al alloy without Ga (Zhuang, et al., 2021). The lower mass-loss rate indicates that the Ga element has higher hydrogen evolution over-potential that can suppress the HER resulting in a slower self-corrosion of the anode (Zhuang, et al., 2021). In other words, the higher discharge voltage implies that the Ga element can reduce the oxide film resistance and accelerate the dissolution of aluminium (Zhuang, et al., 2021).

Apart from the Ga element, researchers also study the influence of zinc (Zn) and indium (In) elements in aluminium alloy. Park et al. (2017) have

compared the battery performance and corrosion rate using three different anodes: 4N grade pure aluminium, aluminium-zinc alloy, and aluminium-zinc-indium alloy. The result shows that 4N Al has a slower corrosion rate than Al-Zn-In alloy and Al-Zn alloy (Park, et al., 2017). Park, et al. (2017) explained that this outcome is due to the presence of iron (Fe) and silicon (Si) impurities (also known as the corrosive impurities of aluminium) in both Al-Zn-In and Al-Zn alloy. From the chemical composition of the anode used in the study, the Si and Fe composition in both alloys are relatively higher than the 4N Al. This phenomenon has shown that the influence of Si and Fe on the aluminium self-corrosion rate is more dominant than the Zn in the study (Park, et al., 2017).

2.2.2 Cathode

The cathode is another vital component of a battery. The battery cathode is usually referred to as the air cathode in AABs, and it consists of three layers: the gas diffusion layer, catalytic layer, and current collector (Liu, et al., 2017). Currently, the main obstacles hindering the commercialization of AABs are the issues that arose due to the air cathode design. These issues include sluggish oxygen reduction reaction (ORR) and oxygen evolution reaction (OER), air cathode flooding with electrolyte, carbonate precipitation, and electrolyte drying out (Liu, et al., 2017). According to Liu, et al. (2017), the ORR is the primary cathodic reaction in the AAB system. There are two pathways for the ORR in alkaline solution: the direct four-electron pathway and the successive two-electron pathway (Liu, et al., 2017). Equation (2.2) below expresses the ORR following the direct four-electron pathway, while Equation (2.3) and Equation (2.4) below show the ORR following the successive two-electron pathway in alkaline electrolyte. The ORR occurs directly through the four-electron transfer pathway when Equation (2.3) and Equation (2.4) occur rapidly (Liu, et al., 2017).

$$O_2 + 2H_2O + 4e^- \rightarrow 4OH^- \tag{2.2}$$

$$O_2 + H_2O + 2e^- \rightarrow HO_2^- + OH^- \tag{2.3}$$

$$HO_2^- + H_2O + 2e^- \rightarrow 3OH^- \qquad (2.4)$$
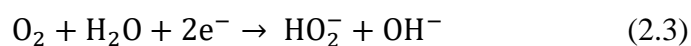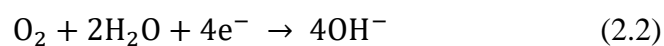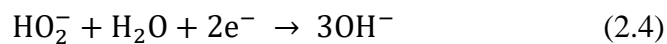
Based on the comprehensive review by Liu, et al. (2017), the issues involving ORR are crucial since the ORR directly affects the performance of the AAB. Hence, researchers have been studying the feasibility of different catalysts to enhance battery performance to overcome the sluggish ORR. The different types of catalysts used to improve the AAB performance include noble metals (platinum and silver), carbonaceous material (also known as carbon-based catalysts), transition metals oxides, and polymer and polymer-based complexes (Goel, et al., 2020). In the literature, Goel, et al. (2020) commented that transition metal oxide and carbon electrodes are better options for AAB because they are naturally abundant (in other words, inexpensive) and follow a four-electron pathway during ORR (Goel, et al., 2020). Furthermore, the electrochemical performance of the cathode with these two catalysts is similar to that Pt/C electrode (Goel, et al., 2020). This literature is highly commendable for providing important information on the available catalyst to overcome the sluggish ORR issue. In addition, the authors also provided the critical insight that transition metal oxide and carbon-based catalyst is more cost-effective than using noble metals for air cathode of AABs.

There are also novels written based on rechargeable AABs. Firstly, Xia, et al. (2020) have used cobalt ion intercalated MnO_2/C as the air cathode for rechargeable AABs. The experiment results show that the 40% Co-MnO_2/C catalyst has the largest specific surface area with 154.25 m^2g^{-1} and the smallest average pore size with a diameter of 6.47 nm among 10%, 20%, 30%, and 50% Co-MnO_2/C catalysts (Xia, et al., 2020). Next, the 40% Co-MnO_2/C catalyst also exhibits the best results in electrochemical measurements. The results show that the 40% Co-MnO_2/C catalyst has the most positive onset potential with 0.859 V, the most positive half-wave potential with 0.727 V, and the highest limiting current density with 4.744 $mAcm^{-2}$ (Xia, et al., 2020). Furthermore, the 40% Co-MnO2/C catalyst has the highest slope value in the Tafel plot (Xia, et al., 2020). These data have indicated that the 40% Co-MnO_2/C catalyst has the best ORR catalytic activity. According to Xia, et al. (2020), the improved catalytic performance in the

ORR is due to the increase in the ratio of Mn^{3+}-Mn^{4+} and hydroxyl absorption oxygen in the catalyst.

For the OER, the 40% Co-MnO_2/C catalyst also exhibits the best results in catalytic performance. The 40% Co-MnO_2/C catalyst yielded the smallest value of onset potential with 1.593 V, the lowest overpotential with 634 mV, and the highest limiting current density with 15.177 $mAcm^{-2}$ (Xia, et al., 2020). In addition, the 40% Co-MnO_2/C catalyst has the smallest slope value with 163 mV/dec in the Tafel plot (Xia, et al., 2020). After that, Xia, et al. (2020) have used the 40% Co-MnO_2/C and MnO_2/C catalysts in rechargeable AAB to conduct a full-cell test. The results show that the 40% Co-MnO_2/C catalyst again has the best cyclic charge and discharge performance. It yielded a battery discharge voltage of above 1 V and a charge voltage of less than 2.5 V during 90 hours of charge and discharge cycle at a limited battery capacity of 375 $mAhg^{-1}$ (Xia, et al., 2020). This experiment by Xia, et al. (2020) has provided a comprehensive examination of the effect of cobalt ions intercalated into MnO_2/C catalysts on the AABs. This experiment also indicates that the specific surface area and the average pore size of the air cathode have a high impact on ORR and OER.

Next, Kuo, et al. (2015) have reported a study to improve the ORR performance using poly-(3,4-ethylenedioxythiophene) (PEDOT) on MnO_2. The MnO_2 have different crystal form and appearance based on its preparation method, the different types of MnO_2 includes alpha (α), beta (β), gamma (γ), and epsilon (ε) (Kuo, et al., 2015). In the study by Kuo, et al. (2015), the types of MnO_2 used are α-MnO_2 and β-MnO_2. After the synthesis of α-MnO_2 and β-MnO_2, the Brunauer-Emmett-Teller (BET) results exhibit that α-MnO_2 has a larger pore size and pore volume than β-MnO_2 with 69.2 nm and 0.369 cm^3g^{-1}, respectively (Kuo, et al., 2015). However, α-MnO_2 has a smaller specific surface area with 22.63 m^2g^{-1} (Kuo, et al., 2015). After that, Kuo, et al. (2015) used linear sweep voltammetry to evaluate the ORR activity of each electrode, and the results show that the PEDOT/α-MnO_2/C electrode achieved the highest current density value with 30.91 $mAcm^{-2}$. This novel by Kuo, et al. (2015) has described that the addition of PEDOT can improve the ORR activity. However, this experiment in this novel in conducted using an alkaline KOH solution which is not rechargeable.

Other than that, Zhang, et al. (2015) have developed an n-type Cu_2O doped activated carbon (AC) as an alternative air cathode. The air cathodes used in the experiment were fabricated using an electrolyte solution of 50 mM copper sulphate and an electrochemical workstation to deposit the copper onto the surface of the AC air cathode. From the experiment results, all the copper electrodeposited (Cu/AC) AC air electrodes yielded a higher current density than pure AC air cathode. These results indicate that the Cu/AC air cathodes have better ORR activity (Zhang, et al., 2015). Furthermore, the open-circuit potentials obtained using Cu/AC air cathodes were between 0.211 V and 0.226 V, which also indicates that the Cu/AC air cathodes have better ORR activity (Zhang, et al., 2015). After that, this literature also shows that the copper electrodeposition on the AC air cathode increases the BET surface area. After that, this literature also shows that the electrodeposition of copper on the AC air cathode increases the BET surface area, the micropore area, the mesopore area, and the total volume of pores. The enlarged surface area improves the ORR activity by providing abundant and high conductivity active sites in the electrochemical reactions.

This literature by Zhang, et al. (2015) is noteworthy in providing a detailed mechanism regarding the addition of copper in improving the ORR activity. This literature also provides another alternative to improve the ORR activity in AABs. Despite the advantages, the experiment in this novel is conducted based on the microbial fuel cell (MFC). The effect of the addition of copper in AABs may be different because different electrolytes are applied. Furthermore, in a rechargeable AAB, the OER is another crucial factor that affects battery performance. As a result, the effect of the copper addition on the OER is unclear.

Next, Li, et al. (2018) have reported a copper-centered metal organic framework (Cu-MOF) derived crystalline Cu/Cu_2O nanoparticles and non-crystalline CuN_xC_y species to modify the Ketjenblack (KB) carbon. For the experiment results, the linear sweep voltammetry curves show that the copper-based nanoparticles modified KB catalyst (CuNC/KB) with a KB mass of 400 mg exhibits the best ORR activity with a half-wave potential of 0.82 V and a limiting current density of 6.05 $mAcm^{-2}$ (Li, et al., 2018). Li, et al. (2018) suggest that these results may be attributed to the enhanced BET surface area

and electronic conductivity. To further confirm the effect of the copper-based nanoparticles in CuNC/KB, the copper-based nanoparticle is removed using hot acid. Consequently, the results show that CuNC/KB after removing the copper-based nanoparticles yielded a weaker ORR activity (Li, et al., 2018). This further implies the importance of the copper-based nanoparticles in the ORR activity. For durability, the change in the half-wave potential after two-thousand cycles for CuNC/KB is only 5 mV, while the change for platinum/carbon is 35 mV (Li, et al., 2018). This research by Li, et al. (2018) is highly advantageous in demonstrating that copper-based nanoparticles can improve the ORR activity as compared to the platinum/carbon.

Apart from transition metals, noble metals such as platinum (Pt), palladium (Pd), iridium (Ir), and ruthenium (Ru) are also identified as highly active OER electrocatalysts due to their low OER overpotential (Vazhayil, et al., 2021). For research regarding noble metals on AABs, Sun, et al. (2016) have fabricated a hybrid catalyst of manganese oxide decorated with silver nanoparticles (Ag-MnO). From the experiment results, the discharge curves with the hybrid catalyst exhibited 199 mAcm^{-2} when the voltage was at 1 V (Sun, et al., 2016). Furthermore, the hybrid catalyst also yielded the maximum power density of 204 mWcm^{-2} (Sun, et al., 2016). This novel by Sun, et al. (2016) has provided an innovative way to reduce the use of noble metal while increasing the AAB performance. However, this experiment was conducted based on primary AAB by using the KOH aqueous solution. Thus, the results may be different on the rechargeable AABs. Furthermore, the experiment conducted by Sun, et al. (2016) also did not consider the effect of the hybrid catalyst on the OER activity.

Next, Luo, et al. (2021) also have fabricated a catalyst using gold-platinum nanoparticles on multi-walled carbon nanotubes for AABs. In this study, different catalysts with different gold-platinum ratios are produced in order to provide different samples for comparisons. The experiment results show that gold-platinum with a ratio of 1.68 has exhibits higher powder density, higher specific capacity, and better durability than other gold-platinum catalysts and platinum-carbon catalysts (Luo, et al., 2021). The results also show that the gold-platinum catalyst can enhance the catalytic performance towards ORR (Luo, et al., 2021). This literature by Luo, et al.

(2021) again demonstrated the strong catalytic performance of noble metals. Mixing noble metals under a specific ratio can further enhance the catalytic performance and the durability of the AABs. As for the disadvantages, this approach may have provided a strong and stable battery performance. However, the formation of the catalyst using noble metals is expensive and uneconomical. Therefore, this approach is not suitable for the commercialization of AABs. Furthermore, the effect of gold-platinum catalysts on OER is not examined during this experiment.

Other than studies on the cathode materials to improve the ORR and OER performance, Mori (2017b) has researched the use of non-oxide ceramic materials as air cathodes to suppress the formation of byproducts such as $Al(OH)_3$ and Al_2O_3. The non-oxide ceramic materials used in the experiment are titanium nitride (TiN), titanium carbide (TiC), and titanium diboride (TiB_2). The cyclic voltammetry shows that the TiC and TiN have stable cyclic performance (Mori, 2017b). The charge-discharge curve of the rechargeable AAB with TiC cathode further demonstrated the stable cyclic performance (Mori, 2017b). After that, the X-Ray Diffusion (XRD) patterns for the aluminium anode and air cathode are obtained with different air cathode as the manipulating variables to evaluate the byproducts suppression. The $Al(OH)_3$ and Al_2O_3 byproducts are not observable in the XRD pattern for the aluminium anode. However, the $Al(OH)_3$ and Al_2O_3 byproducts are detectable in the XRD pattern for the air cathode (Mori, 2017b). According to Mori (2017b), the XRD pattern for air cathode suggests that the $Al(OH)_3$ byproduct forms at all types of air cathode used in the experiment, while the Al_2O_3 byproduct can be found only at TiN and TiN-C air cathode.

Mori (2017b) has further examined the TiC and TiC-C air cathode under X-Ray Photoelectron Spectroscopy (XPS). In contrast with XDR results, the XPS results show that although the XRD patterns cannot detect the Al_2O_3 byproduct, this byproduct exists on the TiC air cathode after the electrochemical reaction (Mori, 2017b). Mori (2017b) has suggested that these byproducts may originate from using the carbonaceous material as the air cathode. He also recommended that the accumulation of the byproducts needs to be further studied to reach a reasonable finding. This literature by Mori (2017b) is highly commendable because his research not only has provided a

solution to a rechargeable AAB with better cyclic performance, it also demonstrates the limitation of XRD. Mori (2017b) also has provided a significant insight that the formation of byproducts may originate from the carbonaceous material from the air cathode. Furthermore, although the non-oxide ceramics cannot thoroughly eliminate the byproducts formation, they can reduce the side reactions and exhibits better battery performance.

After that, Mori (2017a) have used aluminium terephthalate (AT) as a metal-organic framework (MOF) as the air cathode material for rechargeable AABs. In this experiment, an activated carbon was used as the air cathode for benchmarking comparison. He also synthesized another air cathode using AT with conductive carbon (ATCC) to provide another sample for comparison. From the experiment results, the $Al(OH)_3$ and Al_2O_3 byproducts that inhibit the long-term operations of the AAB are undetected from the XRD patterns (Mori, 2017a). For XPS results, the formation of $Al(OH)_3$ and Al_2O_3 byproducts is hard to determine and evaluate from the graph (Mori, 2017a). Although byproducts suppression cannot be identified based on the XPS results, the XDS results imply that the MOF hindered the formation of byproducts during the crystalline phase. From this experiment, even though MOF can inhibit the formation of byproducts, the battery capacity and electrical output were lower than using the AC as the air cathode. Mori (2017a) also found that interfacial cell impedance of MOF as air cathode does not increase even after a long period of electrochemical reactions. This research by Mori (2017a) is advantageous because it has given another solution on byproducts suppression. However, this solution has led to a weaker battery electrical output.

After the catalyst, the catalyst binder is another essential element to fabricate the air cathode. Catalyst binder binds the catalyst powder together and forms paste which can be applied onto the current collector and acting as the catalyst layer of the air cathode. In addition, the catalyst binder also binds the catalyst layer onto the current collector. First of all, Nafion solution is used as the binder for air cathode in MFCs application. Liu, et al. (2012) have prepared two air cathode in their study to compare the effect of different binder. The binder used in their study includes PTFE binder and Nafion binder. From the results, the wet proofed air cathode (with PTFE binder) has

significantly better performance than the non-wet proofed air cathode (with Nafion binder) in terms of power density, electrode potential (Liu, et al., 2012). This study by Liu, et al. (2012) shows the importance of employing the wet proofing properties into the air cathode in enhancing the stability and performance of the air cathode.

After that, Cheng and Wu (2013) have used PTFE as the catalyst binder for MFCs. According to Cheng and Wu (2013), the air cathode catalyst layer was prepared by mixing the 0.8 mg of catalyst mixture, 6 mg PTFE, and 40 μL isopropyl alcohol (IPA) together. The mixture is later pasted onto the current collector and subsequently heated at 370 °C for 30 minutes (Cheng & Wu, 2013). This article by Cheng and Wu (2013) is favourable because it provides detailed air cathode fabrication process. Also, this article discusses the disadvantage of PTFE as binder, that is PTFE is a non-conductive material. This causes coating the PTFE onto the surface of the current collector increases the electric resistance between the current collector and the catalyst layer (Cheng & Wu, 2013). Other than this disadvantages, the PTFE binder actually provides corrosion inhibition efficiency of 97%, which provides sustainability and durability of the air cathode (Liu, et al., 2012).

2.2.3 Electrolyte

As one of the main components that allow electrochemical reactions, the electrolyte is also one of the research topics in AABs. Buckingham, et al. (2021) have grouped electrolytes into two categories: aqueous and non-aqueous electrolytes. Firstly, there are three different aqueous electrolytes based on their pH values: acid electrolytes, neutral electrolytes, and alkaline electrolytes. Alkaline electrolytes are the most commonly used aqueous electrolytes due to their higher theoretical cell potential and achievable power than acid and neutral electrolytes (Buckingham, et al., 2021). Alternatively, the non-aqueous electrolytes include ionic liquids (ILs), solid electrolytes, and semi-solid electrolytes. For non-aqueous electrolytes, Buckingham, et al. (2021) proposed that the two motivations in promoting the research in non-aqueous electrolytes are to avoid the corrosion mechanism in the aqueous electrolytes and to discover the feasibility to develop rechargeable AABs. Buckingham, et al. (2021) also stated that the rechargeability of the AABs

cannot be realized in aqueous electrolytes because the HER will occur before the aluminium deposition. The comprehensive discussion of Buckingham, et al. (2021) has suggested that research in non-aqueous electrolytes is a feasible solution in the development of rechargeable AABs.

As discussed in the previous paragraph, aluminium deposition is the crucial reaction that enables the rechargeability of AABs. Thus, it is required for the non-aqueous electrolytes to be used in rechargeable AABs to consist of ions that allow the deposition of aluminium. Revel, et al. (2014) have discussed that the aluminium deposition reaction can occur by discharging one of the two aluminium-containing complexes: $AlCl_4^-$ and $Al_2Cl_7^-$ anions. Equation (2.5) and Equation (2.6) below display the aluminium deposition from the two aluminium-containing complexes, $AlCl_4^-$ and $Al_2Cl_7^-$ anions, respectively. Subsequently, Revel, et al. (2014) studied the characteristics of different pH values of $AlCl_3$-EMImCl melts as ILs. The cyclic voltammetry obtained indicates that $AlCl_4^-$ and $Al_2Cl_7^-$ are the predominant anions in the acidic melt (Revel, et al., 2014). After that, Revel, et al. (2014) have conducted the half-cell characterization, and the result shows that alkaline and neutral melts undergo nickel solubilization and form blue colour $(EMImCl)_2(NiCl_4)$ cation (Revel, et al., 2014). This research has demonstrated the feasibility of using $AlCl_3$-EMImCl melts as ionic liquids as electrolytes for AABs. However, the experiment does not prove the aluminium deposition.

$$AlCl_4^- + 3e^- \leftrightarrow Al + 4Cl^- \qquad (2.5)$$

$$4Al_2Cl_7^- + 3e^- \leftrightarrow Al + 4AlCl_4^- \qquad (2.6)$$
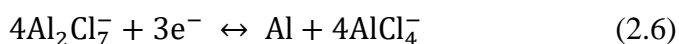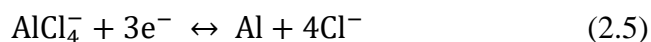
In further studies regarding ILs on secondary AABs, Bogolowski and Dillet (2018) have synthesized three different $AlCl_3$-based electrolytes to evaluate their feasibility in aluminium deposition, oxygen reduction reaction (ORR), and oxygen evolution reaction (OER). These $AlCl_3$-based electrolytes include $AlCl_3$-EMImCl, $AlCl_3$-acetamide, and $AlCl_3$-urea. From the experiment results, $AlCl_3$-EMImCl has the fastest aluminium deposition and the highest current densities (Bogolowski & Drillet, 2018). After evaluating the secondary AABs under half-cell conditions, Bogolowski and Dillet (2018)

further the experiment under full-cell conditions. This result shows that despite AlCl$_3$-EMImCl having better half-cell performance, AlCl$_3$-acetamide and AlCl$_3$-urea have better current and energy efficiency in fullcell conditions (Bogolowski & Drillet, 2018). The experiment conducted by Bogolowski and Dillet (2018) is highly commendable for providing important information on aluminium deposition. This study also suggests that AlCl$_3$-based ILs electrolytes provide the rechargeability of AABs. Other than that, Bogolowski and Dillet (2018) have also provided Pt/C gas diffusion activity for ORR and OER using the three electrolytes on cyclic voltammograms.

After understanding the feasibility of using AlCl$_3$-containing ionic liquids as the electrolyte in rechargeable AABs, researchers have studied the feasibility of gel electrolytes to overcome the air cathode leaking issue. Liu, et al. (2021) have researched using polyamide (PA)-based gel polymer electrolyte (PAGPE) to evaluate the feasibility of gel-based electrolytes. In the research, different molar ratios of AlCl$_3$-EMImCl (1.3:1, 1.5:1, 1.7:1, and 2:1) are mixed with PA to produce different PAGPE. The research result shows that PAGPE with AlCl$_3$-EMImCl with a molar ratio of 1.7:1 exhibits discharge capacities of 90.4, 90.2, 89.6, 88.2, and 68.2 mAg^{-1} at the current densities of 100, 200, 500, 1000, 2000 mAg^{-1}, respectively (Liu, et al., 2021). Furthermore, the same PAGPE exhibits a discharge capacity of 92.8 mAg^{-1} after the current density has returned from 2000 to 100 mAg^{-1} (Liu, et al., 2021). This result indicates that the PAGPE with AlCl$_3$-EMImCl with a molar ratio of 1.7:1 has the best stability in discharge capacity. However, the addition of PA into the AlCl$_3$-EMImCl electrolyte lowers the molar ratio of AlCl$_3$ in the electrolyte and causes the ionic conductivity to be lower than the AlCl$_3$-EMImCl ionic liquid electrolyte (Liu, et al., 2021).

After that, another IL electrolyte, the AlCl$_3$ with 1-butyl-3-methylimidazolium chloride is widely used as electrolytes in the secondary rechargeable aluminium battery (RAB) (Wu, et al., 2018). In this literature, Wu, et al. (2018) have also stated that the interface properties of anode and electrolyte are significant for RAB performance. The solid-electrolyte interphase (SEI) layer that forms on the anode surface is essential in improving the cyclic performance of secondary batteries (Wu, et al., 2018). To verify the statement, Wu, et al. (2018) experimented with AlCl$_3$-EMImCl as the

electrolyte in RAB to evaluate the cyclic performance between treated and non-treated aluminium anode. The experiment result displays the discharge capacity for pre-treated 6 hours aluminium anode exceeds 100 mAh/g rapidly and stabilizes at around 50 mAh/g after thirty cycles (Wu, et al., 2018). For comparison, the untreated aluminium anode breaks down after five cycles (Wu, et al., 2018). This study executed by Wu, et al. (2018) provides an innovative way to stabilize the cyclic performance of rechargeable batteries by reducing the pitting corrosion of anode using appropriate treatment and electrolytes. However, the experiment was conducted based on aluminium-ion batteries, not AABs.

After that, Gelman, et al. (2017) proposed utilizing 1-ethyl-3-methylimidazolium oligofluorohydrogenate [EMIm(HF)2.3F] (another ILs) as the electrolyte for a durable AAB. According to Gelman, et al. (2017), the result of the experiment suggests that the aluminium anode will interact with EMIm(HF)2.3F electrolyte and forms an Al-O-F layer on the anode surface, the formation of the Al-O-F layer enables the activation and low corrosion rates of the aluminium anode (Gelman, et al., 2017). Gelman, et al. (2017) also experimented with the EMIm(HF)2.3F electrolyte under the full-cell conditions. The AAB discharge profiles displayed in the report indicate that the voltage stabilizes for more than 100 hours (Gelman, et al., 2017). From the second part of the research, the data proves that EMIm(HF)2.3F as the electrolyte of primary AAB provides durability and stability of the battery. However, this research does not include the ability of the electrolyte in aluminium deposition and rechargeability. Furthermore, the application of EMIm(HF)2.3F as the electrolyte to provide durability and stability for secondary AAB is also questionable.

For non-aqueous electrolytes, researchers also study the feasibility of solid electrolytes in secondary AABs. Mori (2019) has reported an experiment using a solid electrolyte in rechargeable AAB. The solid-state electrolyte was synthesized using AlCl₃, urea, carboxymethyl cellulose (CMC), and glycerin with a molar ratio of 3:2:1:1. In the results, cyclic voltammetry and charge-discharge curve indicate that the solid electrolyte produced is feasible to be utilized in rechargeable AABs (Mori, 2019). The results also show a stable battery performance (Mori, 2019). Mori (2019) also suggests elucidating the

molar ratio of AlCl$_3$-urea-CMC-glycerin in further studies to enhance battery performance. In this literature, the solid electrolyte applies the AlCl$_3$ solution to provide ions for the electrodeposition of aluminium. This research by Mori (2019) also has provided another solution to eliminate the formation of byproducts and enable stable battery performance. In this literature, the author did not collect the data for a liquid electrolyte for comparison under the same experimental conditions. Although data from other literature is provided in the discussion, the result may vary due to different experimental conditions.

2.2.4   Separator

Other than the three main components (anode, cathode, and electrolyte), a battery separator is also an essential component that affects the performance of a battery. According to Zhang (2007), the primary function of a battery separator is to prevent physical contact between the anode and cathode. Although the battery separator does not participate in the anodic and cathodic reactions of the battery, its structural properties will affect the battery performance in terms of energy and power densities, cycle life, and safety (Zhang, 2007). Thus, there are many studies to research the effect of properties of battery separators on battery performance. According to Luo, et al. (2021), many factors should be assessed and considered before choosing an appropriate battery separator for rechargeable air batteries. These properties include good electronic insulation, optimum pore size and porosity, high chemical and electrochemical stability, excellent wettability to the electrolyte, good mechanical properties, good robust stability and integrity within the space, good thermal stability, and low cost for large-scale industrial production (Luo, et al., 2021).

The chemical and electrochemical stability refers to the corrosion resistance and the expansion and contraction rate of the separator in the electrolyte for a certain period (Luo, et al., 2021). Next, the wettability refers to the ability of the separator to absorb liquids (Luo, et al., 2021). As for the mechanical properties, it refers to the puncture strength and tensile strength of the separator (Luo, et al., 2021). In this literature, Luo, et al. (2021) have listed out all the separator parameters that have impact on the battery performance. They also have provided a value for each of the parameters for benchmarking.

However, the weakness of this literature is that the general requirement for each parameters provided are based on rechargeable batteries only. The type of the rechargeable battery is not provided in the novel.

Other than review on the battery separator properties that may affects the battery performance, Luo, et al. (2021) also highlight the different types of the separator that are presently used. First of all, the microporous polymer membranes are the simplest battery separator which is fabricated using polymers such as polyethylene (PE), polypropylene (PP), polystyrene (PS), polyoxymethylene (POM), and polyethylene terephthalate (PET) as the raw material. The second type of separator is categorized as the modified microporous polymer membranes. There are many methods to modify the polymer membranes, these methods include surface coating modification, surface grafting modification, blending modification, and multilayer modification. After that, the third type of battery separator is the non-woven membrane (also known as the fibrous membrane) that is produced using mechanical, physical, or chemical interactions to binds multiple fibers together (Luo, et al., 2021).

As for the fourth battery separator, the cellulose-based membranes are fabricated using the natural biomass polymer compound known as the cellulose (Luo, et al., 2021). According to Luo, et al. (2021), the cellulose is also an important raw material in the paper industry. Thus, the are some homemade AABs using papers or tissues as the battery separator. Lastly, the electrolyte membranes are solid-state electrolytes that functions as both battery separator and electrolyte. The examples of electrolyte membranes are the solid ceramic electrolyte, the solid polymer electrolyte, gel polymer electrolyte, and composite electrolyte. This literature by Luo, et al. (2021) is highly significant that it provides a comprehensive discussion the battery separator for rechargeable battery. This literature not only discuss on the essential parameters of the battery separators, it also mentions the various studies done by researchers on the battery separator. Furthermore, this novel provides the different types of battery separator that have been experimented by researchers.

Next, Nguyen, et al. (2014) have made a review regarding the paper-based batteries. The motivation to paper-based batteries is due to the extremely cheap, commercially available, thin, lightweight, flexible, biocompatible, and

biodegradable of paper (Nguyen, et al., 2014). In this review by Nguyen, et al. (2014), the literature shows that most paper-based batteries apply the paper as the reservoir for electrolyte. Other than acting as the reservoir for electrolyte, the paper also functions as the battery separator (Nguyen, et al., 2014). The review article is advantageous in that providing various research regarding paper-based batteries. Although there is no paper-based AAB being reviewed in this article, it provides an insight in the development of small and compact battery for research. In addition, this novel also shows the feasibility of paper as the cellulose membrane for the application as battery separator. On the other hand, porous water-based filter membrane is also applicable as battery separator (Qin, et al., 2020).

After that, Tan, et al. (2021) have developed an AAB using polypropylene (PP) absorbent pad and Kimwipes as the battery separator. The Kimwipes used in this study is another cellulose-based separator. From the experiment results, the PP separator exhibits a better battery performance than the cellulose-based separator. Tan, et al. (2021) explains that the cellulose-based separator swells when immersed in the electrolyte while the fiber-based separator (PP separator) remains unchanged when immersed in the electrolyte. The swelling of the separator changes the electrochemical properties of the separator that affects the battery performance (Tan, et al., 2021). This article by Tan, et al. (2021) is noteworthy in that providing the stability of fiber-based and cellulose-based separator in AAB using potassium hydroxide (KOH) electrolyte. This research by Tan, et al. (2021) also shows another example of paper-based AAB.

For research regarding separators in the $AlCl_3$ electrolyte, Elia, et al. (2017) have developed polyacrylonitrile (PAN) separator for aluminium batteries. They also used some commercially available separators in the experiment for comparisons. First of all, in the electrochemical stability test based on the mass loss of the separator after full immersion in the $AlCl_3$-EMImCl electrolyte, the combination of polyethylene/polypropylene with polyvinyl alcohol micorfibers and nanofibers (PE/PP + PVA) yielded a zero percent mass loss (Elia, et al., 2017). Elia, et al. (2017) explains that the zero-mass loss may due to the presence of PVA. However, the colour change of the separator suggest that the separator is instable. After the PE/PP + PVA

separator, the glass fiber exhibits a 1.2% of minor mass loss and does not have visually observable changes after full immersion in the electrolyte (Elia, et al., 2017). Thus, the glass fiber separators are considered as the most suitable separator for aluminium batteries among other commercially available separators. As for the developed PAN separator, the results show that it is stable in the $AlCl_3$-EMImCl electrolyte (Elia, et al., 2017). The results also suggest that the PAN separator leads to a more homogeneous aluminium deposition (Elia, et al., 2017). This literature has shown an innovative way in determine the electrochemical stability of separators. In addition, this novel also shows that non-woven membranes (glass fiber membrane and PAN membrane) as the aluminium battery separator is electrochemically stable.

2.3 Summary

All the functional components of the AABs have different challenges that discourage the commercialization of AABs. As a result, several researchers have been studying the issues faced by the AABs in an effort to promote green energy. For the anode, the problems include surface passivation and hydrogen evolution. It was also found that the hydrogen evolution issue only occurs on primary AABs that use alkaline KOH. This issue does not happen on the secondary AABs that use $AlCl_3$-based electrolytes. As for the cathode, the ORR and OER remain the most critical challenges. Researchers have been conducted experiments with different approaches to improve the rate of ORR and OER. Thirdly, for electrolytes, it was found that the alkaline aqueous KOH solution is infeasible for the application of secondary AABs. Only ionic liquids (ILs) containing $AlCl_3$ is applicable due to their ability to enable the aluminium electrodeposition. Thus, researchers have been investigating the feasibility of other ILs in the rechargeable AABs. Finally, battery separators which are essential for small-sized batteries also may affects the performance of the AAB. Despite it is not necessary for bulky batteries, there are still many studies regarding this battery separator because smart devices such as smartphones and laptops requires the small-sized paper-based battery.

CHAPTER 3

METHODOLOGY AND WORK PLAN

3.1   Introduction

This chapter shows the materials and equipment required for the study. The fabrication process of the rechargeable AAB and the assembly procedure are also explained in this chapter. Lastly, the work plan is scheduled using a Gantt chart is shown in this chapter too. The flowchart for the methodology and work plan is shown in Figure 3.1.
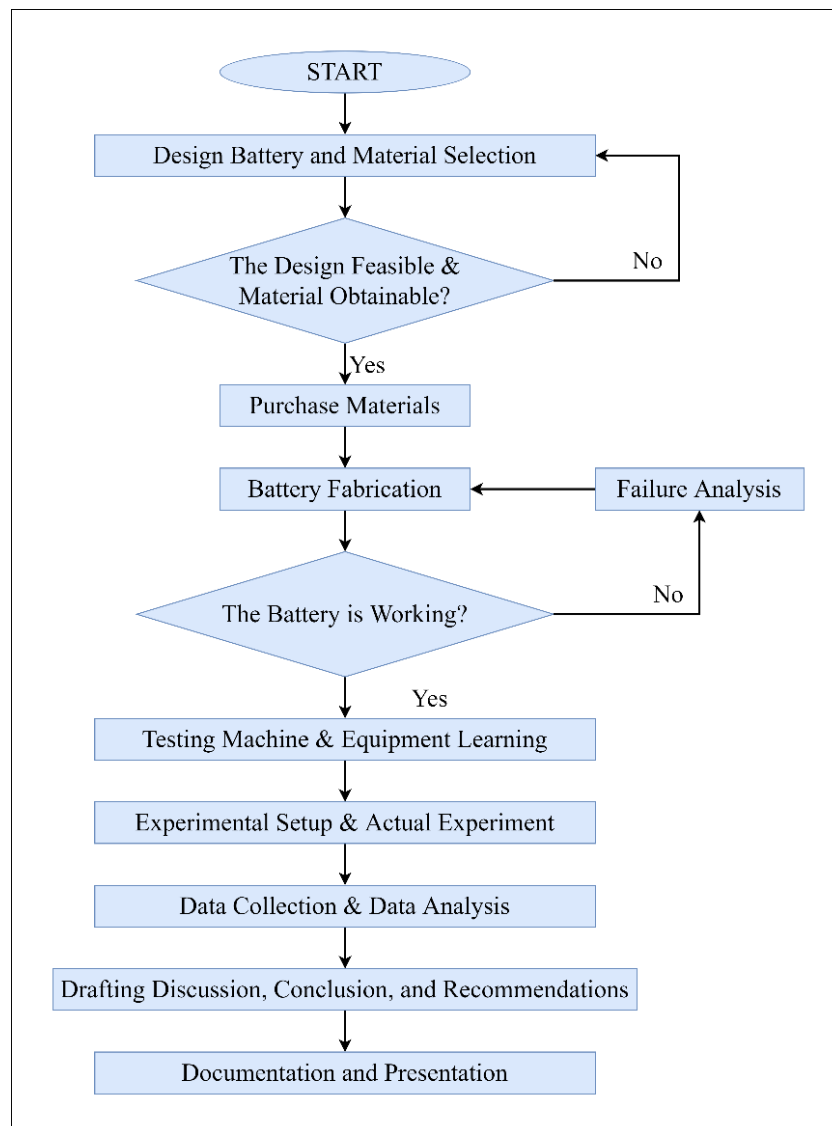
Figure 3.1: Methodology and work plan flowchart.

3.2 Materials Preparation

Aluminium from commercial kitchen aluminium foil was used as the battery anode. Next, the air cathode consists of pure nickel mesh as current collector, 10% (w/v) PVDF solution as catalyst binder using PVDF powder and dimethyl sulfoxide (DMSO), and catalyst mixture of activated carbon (AC), carbon black (CB), and reduced graphene oxide (rGO). For the electrolyte, potassium hydroxide (KOH) is used to make the aqueous electrolyte and Ethyl Acetate are used as the additives. Finally, battery separator used in this study are glass fiber filter membrane and laboratory filter paper.

3.3 Aluminium-Air Battery Design

The AAB design to be used for this project is shown in Figure 3.5 below. For the housing material selection, the acrylic with transparent and inert properties are chosen. For the manufacturing process, the acrylic sheet with 10 mm thickness was purchased and milled using CNC milling machine.
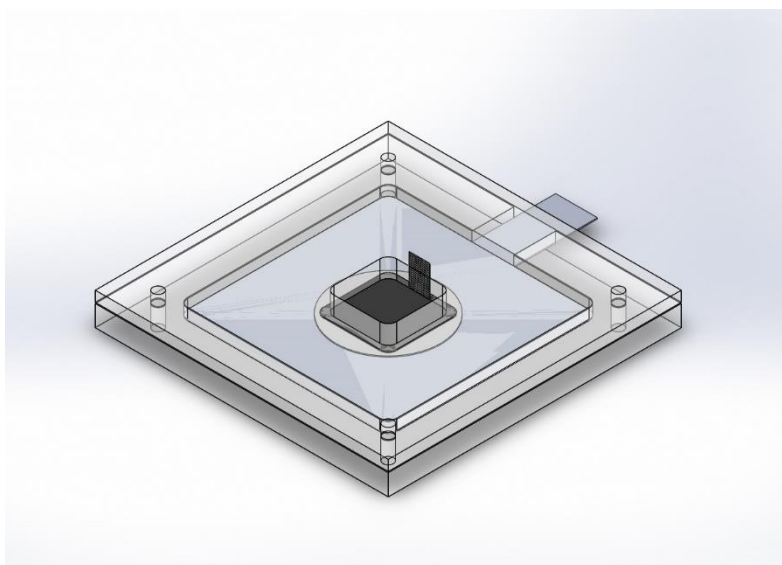
Figure 3.2: AAB conceptual design.

According to Figure 3.2, the AAB housing consists of two parts, the upper housing and the lower housing. The CAD drawings of the housing are also shown in Figure 3.3 and Figure 3.4 below. There are 4 through holes located at each corner of the both housings. These holes are for bolt and nut fastening and tighten the contact between the main battery components.
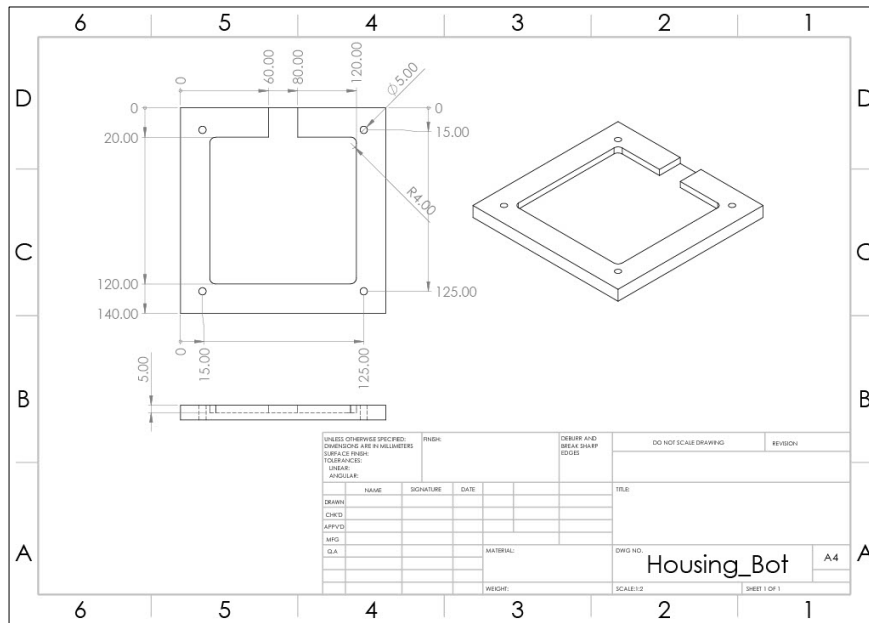
Figure 3.3: Bottom housing CAD drawing.
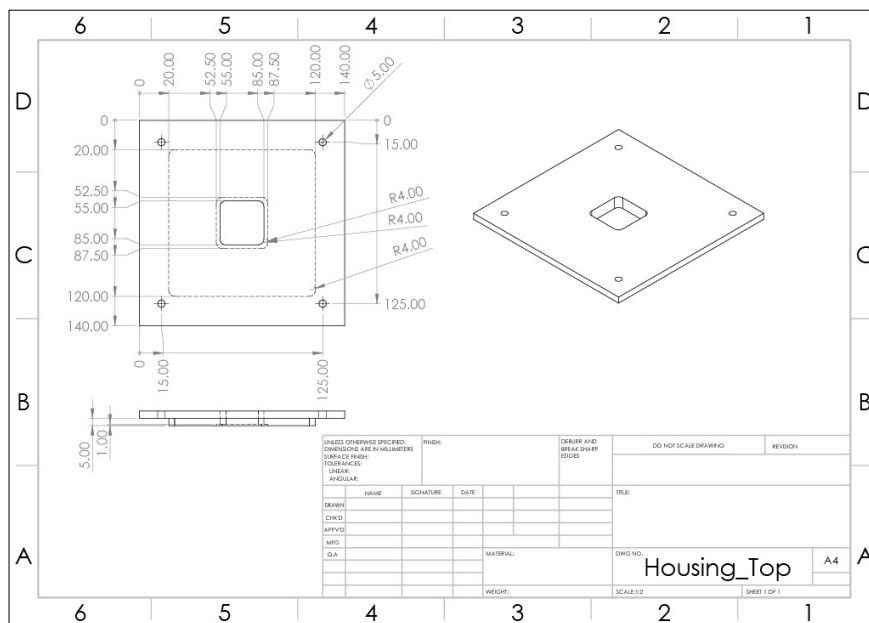
Figure 3.4: Top housing CAD drawing.

3.4   Preparation of Reduced Graphene Oxide

Graphene oxide (GO) powder was thermally reduced at temperature of 350 °C in the furnace (Sengupta, et al., 2018). The GO used heated inside the furnace for 7 minutes (Sengupta, et al., 2020). The obtained rGO after the reduction process was used immediately after it was cool off.

3.5   Air Cathode Fabrication

Firstly, the 10% (w/v) PVDF solution was prepared by mixing 10 mL of DMSO into 1.0 g of PVDF powder. The mixture is stirred using magnetic stirrer at room temperature and 750 rpm for overnight (approximately 16 hours) to completely dissolve the polymer. The preparation process is illustrated in Figure 3.5 below.

After the PVDF solution is ready for use, catalyst mixture consists of 300 mg of AC and 30 mg of CB were mixed and stirred in a beaker. After that, 1 mL of 10% (w/v) PVDF solution is added to the catalyst mixture and stirred using stainless steel spatula. The mixture will become a paste as shown in Figure 3.5 above after the stirring process. The paste was then applied evenly onto the surface of the nickel mesh as shown in Figure 3.5 above.

3.6   Electrolyte Preparation

1M and 4M KOH solution was prepared by mixing the 2.81 g and 11.22 g of KOH pallets with 50 mL of distilled water, respectively. The mixture was stirred until all of the KOH pallets are completely dissolved. Next, 10% (v/v) ethyl-acetate/KOH electrolyte was prepared by mixing 5 mL of ethyl-acetate with 50 mL of 4M KOH solution.

3.7   Aluminium-Air Battery Assembly

After the all the preparations, the developed battery is assembled for performance testing. Figure 3.6 below shows the battery assembly process. From Figure 3.6, Step 1 is to cut the aluminium foil and place the cut foil onto the open pocket of the bottom battery housing. The center of the aluminium can be smaller but need to be greater than the size of the separator. Next, Step 2 is to place and center the separator on the aluminium anode. After positioning the separator, 0.5 mL of electrolyte was added to the separator. Step 3 is to wait the electrolyte to spread and distribute around the separator. After that, Step 4 is to place the air cathode onto the separator, and it is required to make sure that the edge of the cathode is not in contact with the aluminium anode. Finally, Step 5 is to close the upper battery housing can tighten the battery using screws and nuts at the four corners. After that, the

battery is connected to the electrochemical workstation for battery performance testing. The assembly process is repeated for different air cathodes and electrolytes.
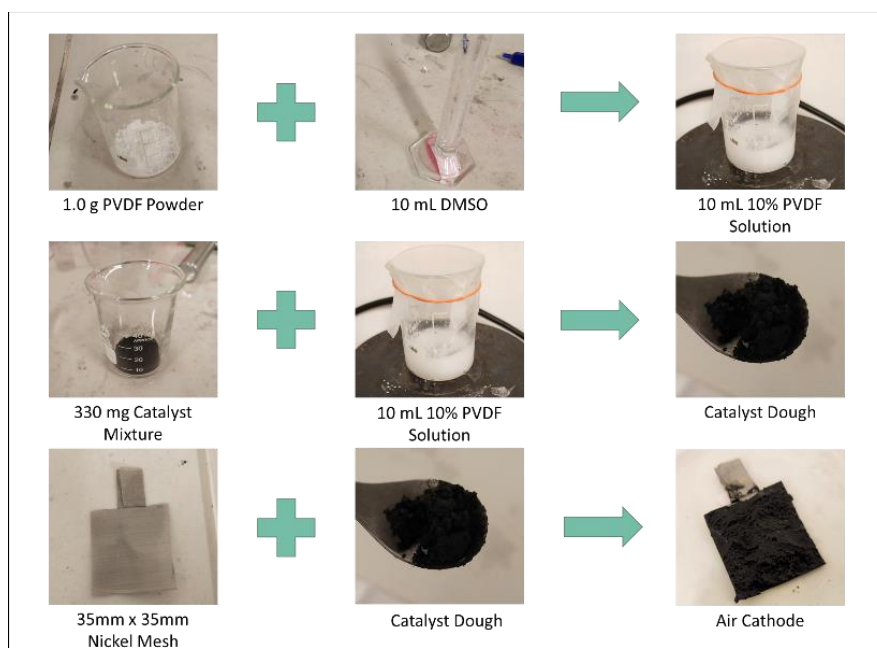
Figure 3.5: Air cathode fabrication.
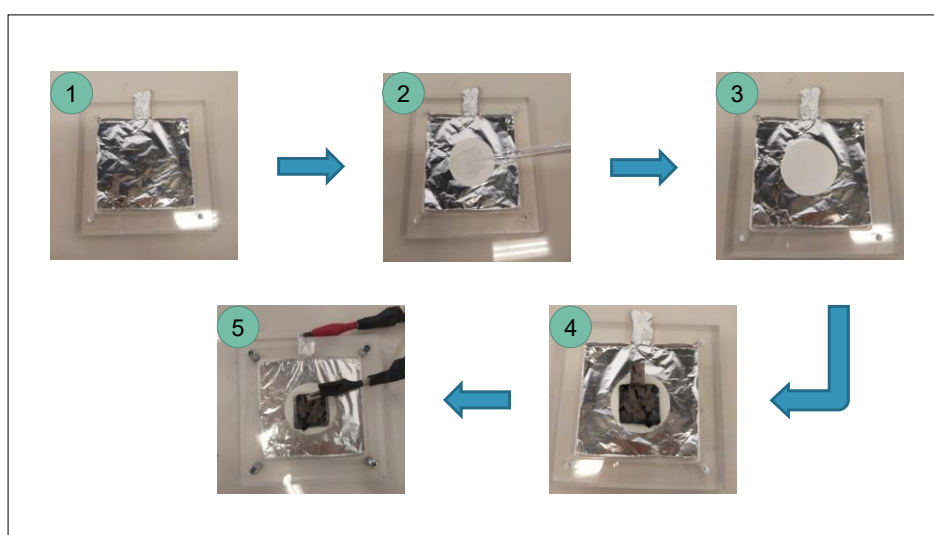
Figure 3.6: Battery assembly process.

3.8   Aluminium-Air Battery Testing

Hitachi S-3400N Scanning Electron Microscope instrument was used to investigate the surface morphologies and element distributions of the aluminium anode and separators through scanning electron microscope (SEM)

and energy dispersive X-ray spectroscopy (EDX) testing. As for the electrochemical workstation, Princeton Applied Research VersaSTAT 4 instrument was used to obtain the charging and discharging performance of the battery. After the testing, the discharge capacity and the energy density of the battery using the Equation (3.1) and Equation (3.2), respectively. The mass loss in Equation (3.2) is referring to the mass loss on the aluminium anode.

$$\text{Discharge Capacity} = \text{Discharge Current} \times \text{Total Time} \qquad (3.1)$$

$$\text{Energy Density} = \frac{\text{Discharge Capacity} \times \text{Average Potential}}{\text{Mass Loss}} \qquad (3.2)$$

As for the experiment inputs, the discharging performance of the AAB is obtained using 10 mA of discharge current and the current discharge operation is to be stopped after the battery potential reached or become smaller than zero. After the preparation on the software, the sensor and working electrodes of electrochemical workstation are connected to the battery anode while the counter and reference electrode are connected to the battery cathode. As for the mass loss of the aluminium anode, the mass of the aluminium was measured each time before the battery assembly and battery testing due to the slight difference in the dimensions of the aluminium sample. The inconsistency of the aluminium sample will not affect the battery performance as the effective reaction area is within the area of contact between the separator and the aluminium anode.

3.9 Gantt Chart

This section displays the Gantt chart used to schedule the battery fabrication plan and battery testing plan during the second final year project semester. The schedule for week 1 until week 7 and the schedule for week 8 until week 14 is shown in Figure 3.7 and Figure 3.8, respectively.

EVALUATE THE CHARGING AND DISCHARGING PERFORMANCE OF THE RECHARGEABLE ALUMINIUM-AIR BATTERY

UNIVERSITI TUNKU ABDUL RAHMAN (UTAR)

Khoo Wen Loong

Project Start: Mon, 13/6/2022
Display Week: 1

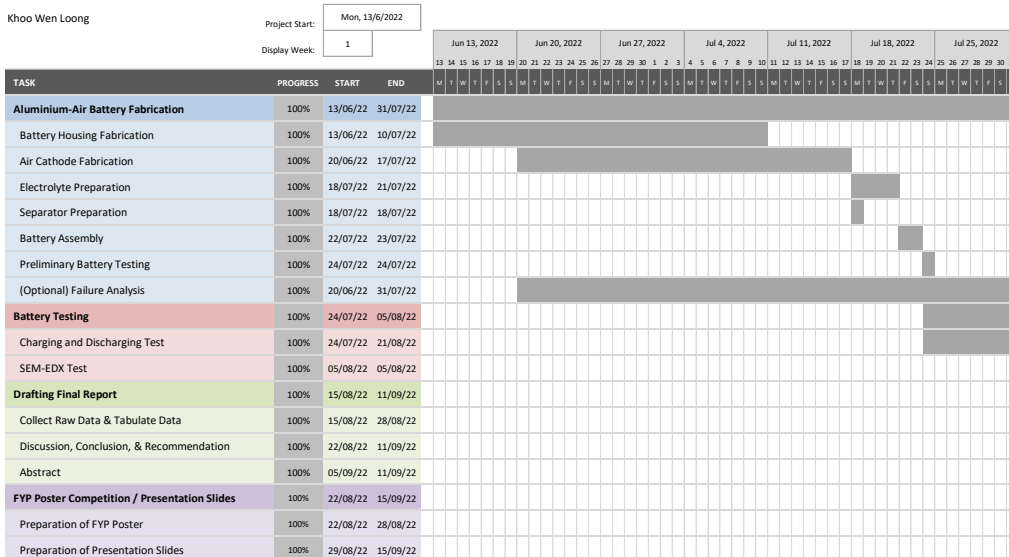| TASK	PROGRESS	START	END	Jun 13, 2022	Jun 20, 2022	Jun 27, 2022	Jul 4, 2022	Jul 11, 2022	Jul 18, 2022	Jul 25, 2022
Aluminium-Air Battery Fabrication	100%	13/06/22	31/07/22							
Battery Housing Fabrication	100%	13/06/22	10/07/22							
Air Cathode Fabrication	100%	20/06/22	17/07/22							
Electrolyte Preparation	100%	18/07/22	21/07/22							
Separator Preparation	100%	18/07/22	18/07/22							
Battery Assembly	100%	22/07/22	23/07/22							
Preliminary Battery Testing	100%	24/07/22	24/07/22							
(Optional) Failure Analysis	100%	20/06/22	31/07/22							
Battery Testing	100%	24/07/22	05/08/22							
Charging and Discharging Test	100%	24/07/22	21/08/22							
SEM-EDX Test	100%	05/08/22	05/08/22							
Drafting Final Report	100%	15/08/22	11/09/22							
Collect Raw Data & Tabulate Data	100%	15/08/22	28/08/22							
Discussion, Conclusion, & Recommendation	100%	22/08/22	11/09/22							
Abstract	100%	05/09/22	11/09/22							
FYP Poster Competition / Presentation Slides	100%	22/08/22	15/09/22							
Preparation of FYP Poster	100%	22/08/22	28/08/22							
Preparation of Presentation Slides	100%	29/08/22	15/09/22							

Figure 3.7: FYP 2 Gantt chart for week 1 until week 7.

EVALUATE THE CHARGING AND DISCHARGING PERFORMANCE OF THE RECHARGEABLE ALUMINIUM-AIR BATTERY

UNIVERSITI TUNKU ABDUL RAHMAN (UTAR)

Khoo Wen Loong

Project Start: Mon, 13/6/2022
Display Week: 8

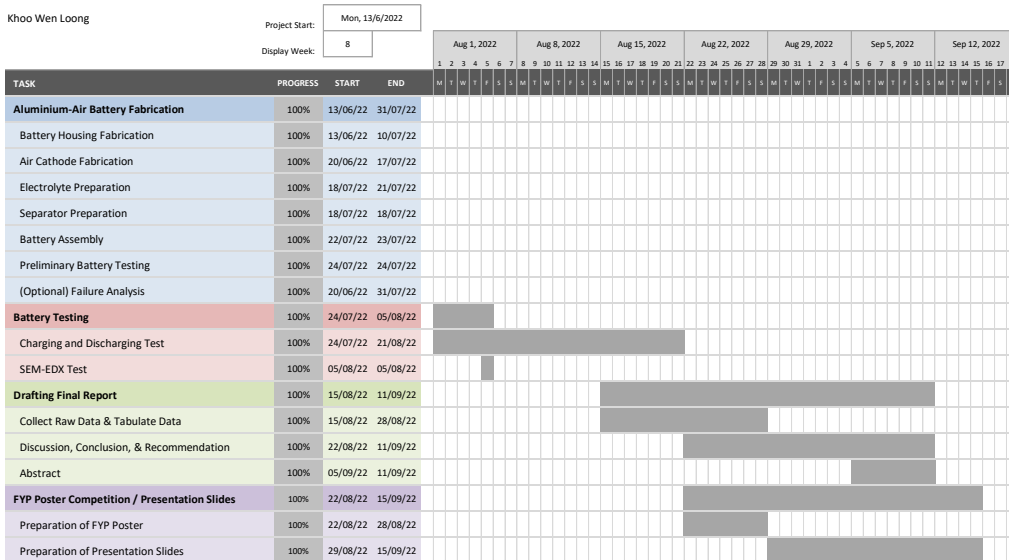| TASK	PROGRESS	START	END	Aug 1, 2022	Aug 8, 2022	Aug 15, 2022	Aug 22, 2022	Aug 29, 2022	Sep 5, 2022	Sep 12, 2022
Aluminium-Air Battery Fabrication	100%	13/06/22	31/07/22							
Battery Housing Fabrication	100%	13/06/22	10/07/22							
Air Cathode Fabrication	100%	20/06/22	17/07/22							
Electrolyte Preparation	100%	18/07/22	21/07/22							
Separator Preparation	100%	18/07/22	18/07/22							
Battery Assembly	100%	22/07/22	23/07/22							
Preliminary Battery Testing	100%	24/07/22	24/07/22							
(Optional) Failure Analysis	100%	20/06/22	31/07/22							
Battery Testing	100%	24/07/22	05/08/22							
Charging and Discharging Test	100%	24/07/22	21/08/22							
SEM-EDX Test	100%	05/08/22	05/08/22							
Drafting Final Report	100%	15/08/22	11/09/22							
Collect Raw Data & Tabulate Data	100%	15/08/22	28/08/22							
Discussion, Conclusion, & Recommendation	100%	22/08/22	11/09/22							
Abstract	100%	05/09/22	11/09/22							
FYP Poster Competition / Presentation Slides	100%	22/08/22	15/09/22							
Preparation of FYP Poster	100%	22/08/22	28/08/22							
Preparation of Presentation Slides	100%	29/08/22	15/09/22							

Figure 3.8: FYP 2 Gantt chart for week 8 until week 14.

CHAPTER 4

RESULTS AND DISCUSSION

4.1   Introduction

This chapter shows the experiment results obtained using the developed aluminium-air battery with different air cathodes, separators and electrolytes. The results are separated into three sections, the electrolyte characterization section, cathode characterization section, and separator characterization section. Each of the section shows only the results that are done to evaluate and analyze the of the specific component on the battery performance.

After that, the by using the components that produces the best battery performance, a charging and discharging performance of the rechargeable aluminium-air battery was obtained and the results was discussed in the last section of this chapter.

4.2   Electrolyte Characterization

The surface morphologies of the aluminium anode before experiment, after experiment with 1M KOH electrolyte, and after experiment with KOH-ethyl acetate electrolyte was investigated using SEM-EDX test. The SEM results for the aluminium samples were arranged and labelled in Figure 4.1 below.
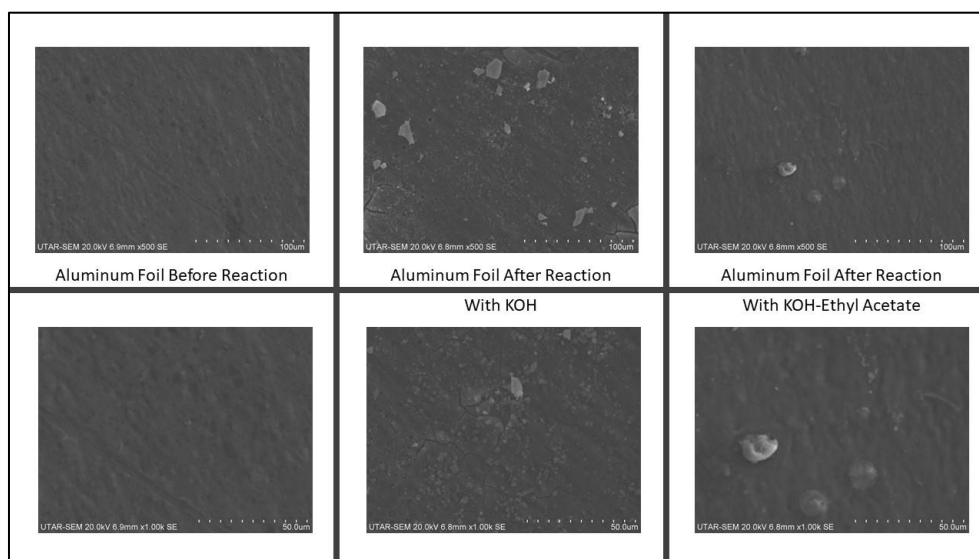

Figure 4.1: SEM results for aluminium samples.

Through observation from Figure 4.1, the surface of the aluminium foil is clean and does not have any surface defects. This sample scanned for providing the initial state of the anode and for comparison with the aluminium foil after the experiment with different electrolyte. After that, for the second sample (aluminium foil after experimenting with 1M KOH electrolyte), the multiple surface defects such as cracks and formation of precipitates can be observed. Lastly, from the third sample (aluminium foil after experimenting with Ethyl-Acetate/KOH electrolyte), the surface has lesser defects as compared to the surface defects found on the second sample. To evaluate the precipitates formed after experiment, EDX test was also performed together with the SEM test. The EDX results obtained shown in Figure 4.2 and the element compositions are tabulated in Table 4.1 below.
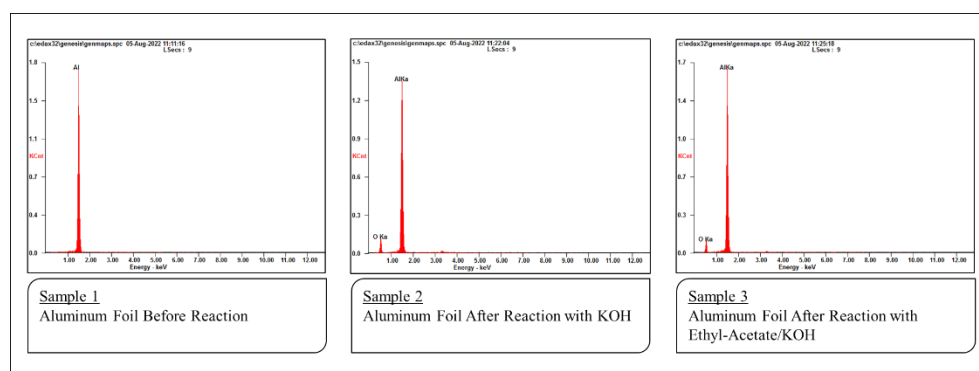

Figure 4.2: EDX results for aluminium samples.

Table 4.1: The element compositions found on aluminium samples.

	Al	O
Sample 1	100.00%	0%
Sample 2	76.14%	23.86%
Sample 3	87.20%	12.80%

From Table 4.1 above, Sample 1 represents aluminium foil before any electrochemical reaction, Sample 2 represents aluminium foil after reaction with KOH electrolyte, and Sample 3 represents aluminium foil after reaction with Ethyl-Acetate/KOH electrolyte. Noting that due to the limitation of the EDX machine, which is the presence and the composition of the hydrogen

element was unable to be evaluated. Thus, the composition results does not show the accurate results regarding the amount $Al(OH)_3$ that is produced. However, the EDX results implies that the precipitates forms on the surface of the aluminium foil may be the $Al(OH)_3$. According to both Figure 4.1 and Figure 4.2, the experiment results show that the addition of additives, which is the ethyl-acetate inhibits and reduces the formation of $Al(OH)_3$.

4.3 Cathode Characterization

Several cathodes are fabricated using different loadings of reduced graphene oxide (rGO) and different mesh size. The labeling of the cathode with the combination of mesh and the composition of the catalyst layer was tabulated in Table 4.2 below. All the 5 cathodes listed in Table 4.2 are assembled into and tested through discharge testing. The discharge performance for cathode with different mesh size is plotted in the graph shown in Figure 4.3 below while the discharge performance for cathode with different rGO loadings are plotted in another graph which is shown in Figure 4.4 below. In another words, Figure 4.3 compares the effect of mesh size on the battery discharge performance with Cathode 1 and Cathode 2, while Figure 4.4 compares the effect of different rGO loadings on the battery discharge performance with Cathode 2, Cathode 3, Cathode 4, and Cathode 5.

Table 4.2: Materials used for different cathode.

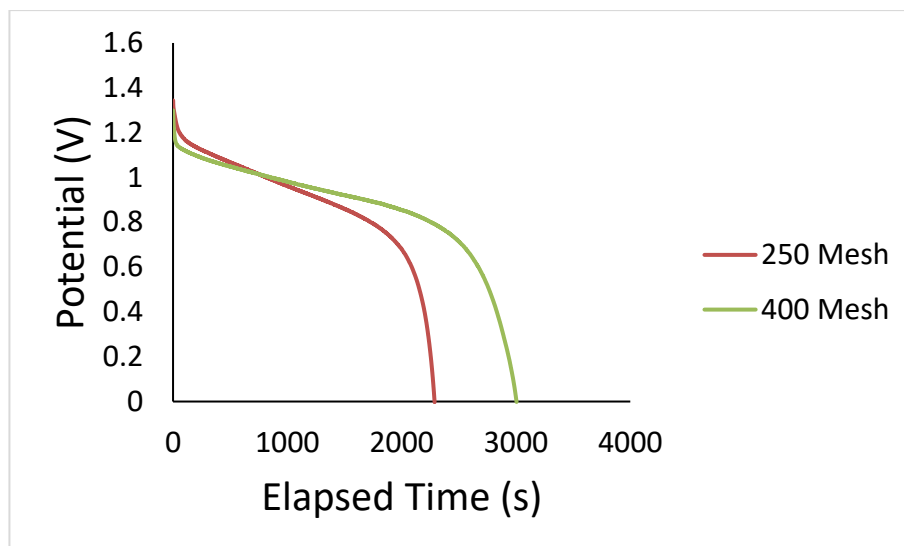| Cathode	Mesh Size	CB	AC	rGO
Cathode 1	250	300 mg	30 mg	0 mg
Cathode 2	400	300 mg	30 mg	0 mg
Cathode 3	400	300 mg	25 mg	5 mg
Cathode 4	400	300 mg	15 mg	15 mg
Cathode 5	400	300 mg	5 mg	25 mg

Figure 4.3: Discharge curve with cathode with different current collector mesh size.
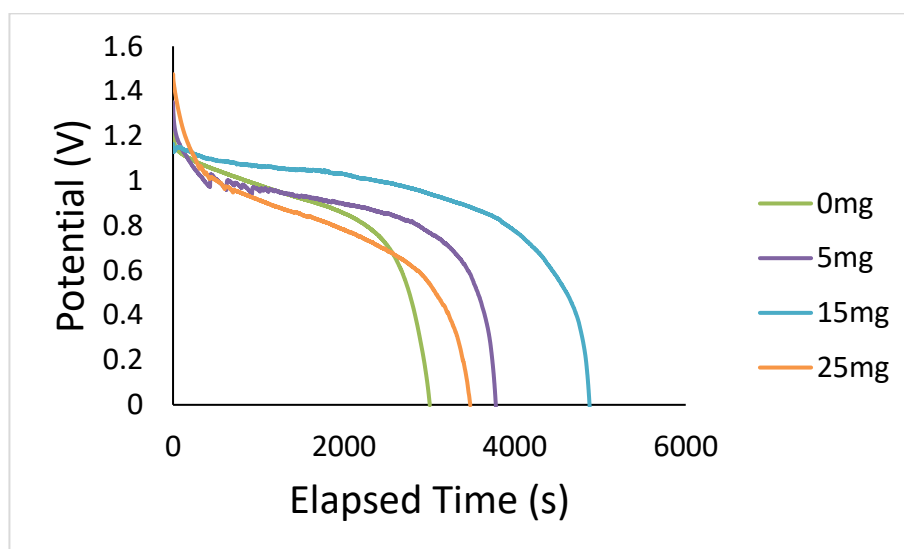

Figure 4.4: Discharge curve with cathode with different rGO loadings.

Firstly, both 250 Mesh and 400 Mesh in Figure 4.3 represents the mesh size of the current collector. They can be interpreted as the number of openings per meter square of mesh. Based on observation from the graph, the results show that the discharge potential for both cathodes are similar, but the time taken for the batteries to complete the discharge test have significant difference. The experiment results implies that the greater the number of openings per meter square of mesh, the greater of the discharge capacity of the battery. Through calculations, the battery with cathode with 250 Mesh and 400

Mesh yielded discharge capacity of 6.36 mWh and 8.35 mWh, respectively. Although there is no third mesh size to show the trend, however, this experiment results corresponds to the experiment results conducted by Janicek, et al. (2015) in MFCs application. Based on their studies, the cathode with higher mesh size has higher maximum power density than cathodes with smaller mesh size. When the mesh size further decreases, the maximum power density further decreases (Janicek, et al., 2015).

Next, Figure 4.4 shows the discharge performance of the battery using cathodes with different rGO loadings. From the graph, it can be observed that all the cathodes with the addition of rGO (Cathode 3, Cathode 4, and Cathode 5) yielded the better discharge performance than the cathode without the addition of rGO (Cathode 1). Through calculations, the battery with cathode with addition of 0 mg, 5 mg, 15 mg, and 25 mg of rGO yielded discharge capacity of 8.35 mWh, 10.49 mWh, 13.54 mWh and 9.66 mWh, respectively. This result implies that the addition of rGO can enhance the battery discharge performance. By comparing only the cathodes with the addition of rGO (Cathode 3, Cathode 4, and Cathode 5), the discharge performance inreases when the rGO loading increases from 5 mg to 15 mg. However, the discharge performance decreases when the rGO loading further increases from 15 mg to 25 mg. This shows the the optimum rGO loading is approximately 4.5%. These experiment results are also tally with the results obtained by Koo, et al. (2019) which is also based of MFCs application. The experiment results show that the power density of exhibited by the cathode decreases in the order of 15 mg, 5 mg, 30 mg, and 0 mg.

4.4   Separator Characterization

To evaluate the effect of different filter paper and glass fiber on the battery performance, the cathode with the best discharge performance, which is the cathode with addition of 15 mg rGO is used to test the battery. The discharge performance of the battery with different separators are plotted in the graph shown in Figure 4.5 below. Other than the electrochemical performance, the surface morphologies of the separators are also investigated using SEM-EDX test. The SEM results to compare the separators are shown in Figure 4.6 below.
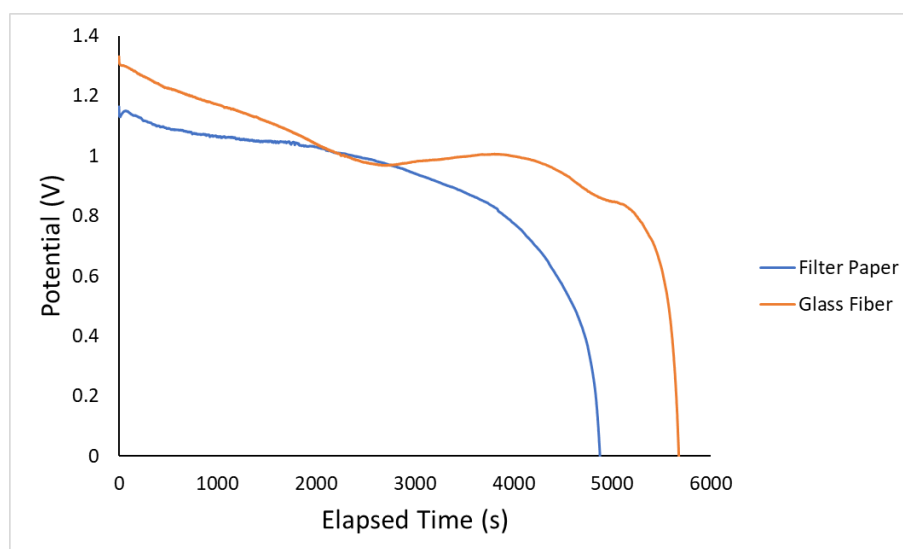
Figure 4.5: Discharge curves with different separator.

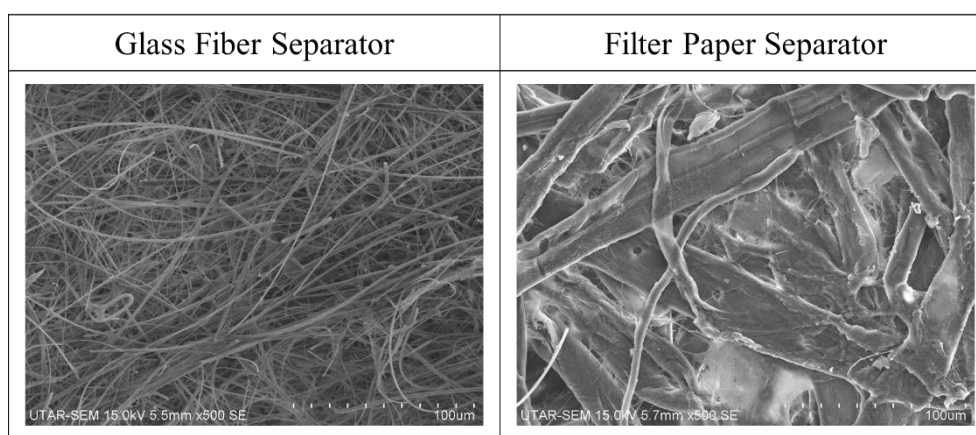| Glass Fiber Separator	Filter Paper Separator

Figure 4.6: SEM results for separators before addition of electrolyte with magnification of x500.

Firstly, by observing the discharge performance plotted in the graph shown in Figure 4.5 above, the glass fiber separator exhibits significantly better discharge performance than the filter paper separator in terms of discharge potential and the discharging time. Through calculations, the discharge capacity obtained using filter paper and glass fiber as separator are 13.54 mWh and 15.76 mWh, respectively. With the best results, the energy density obtained is 297 mWh/g. Next, the surface of both separators is observed from the SEM results under the same magnification as shown in Figure 4.6. Through observations, the glass fiber separator is formed from a matrix of thin and thread-like structures as its name suggests while the filter

paper separator is formed from a matrix of bulky, thick, and flat structures. By relating the SEM images with the discharge curves from Figure 4.5 and Figure 4.6, respectively, the experiment results suggest that the fiber structure of the separator enables better battery discharge capacity. This result is tally with the findings by Elia, et al. (2017) where electrospinning developed non-woven membrane exhibited the best performance.

After that, the EDX results obtained for both separators are compiled in Figure 4.7 below while the element compositions are tabulated in Table 4.3 below. Based on the tabulated data shown in Table 4.3, the commercial cellulose-based filter paper separator only consist of oxygen element and carbon elements, which is also the main element of cellulose $((C_6H_{10}O_5)_n)$. As for the glass fiber separator, other than its main element of silica (SiO_2), there are also many others element that can be found on the separator.

Table 4.3:   The element compositions found on separators.

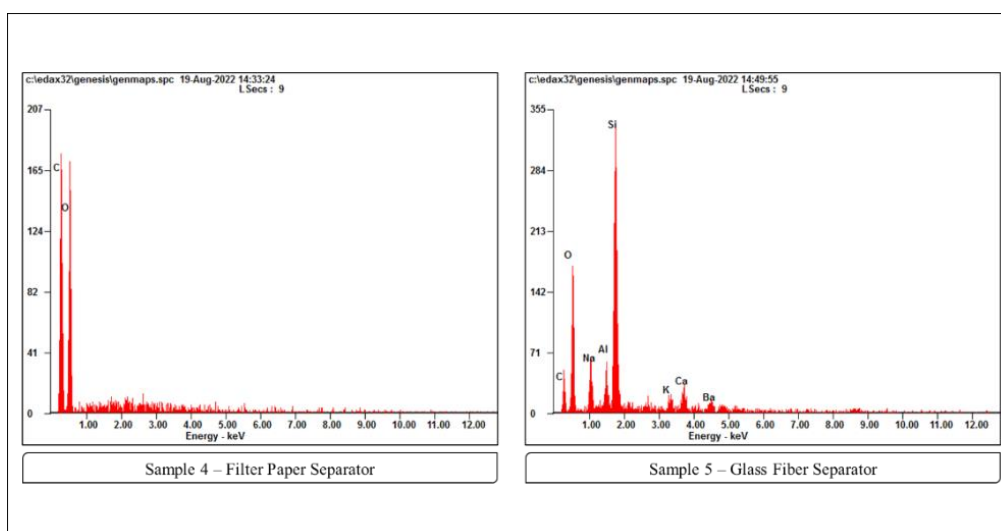|	Sample 4 – Filter Paper	Sample 5 – Glass Fiber
C	47.42%	17.14%
O	52.58%	32.17%
Na	–	06.08%
Al	–	03.76%
Si	–	27.22%
K	–	02.36%
Ca	–	04.02%
Ba	–	07.25%

Figure 4.7: EDX results for separators.

To understand the electrochemical stability of the different separators under the ethyl-acetate/KOH electrolyte, both separators are soaked with the electrolyte and the surface morphologies of the separators before and after the electrochemical reactions are investigated using SEM-EDX test. The SEM results for the separators after soaking with the ethyl-acetate/KOH electrolyte SEM results for the separators after electrochemical reactions are displayed in Figure 4.8 below. As for the EDX results, the results for both separators are tabulated in Table 4.4 and Table 4.5 below. Table 4.4 shows the element compositions found on the surface of the filter paper separator before and after the electrochemical reaction (discharging test), while Table 4.5 shows the element compositions found on the surface of the glass fiber separator before and after the electrochemical reaction.

Table 4.4: EDX results for filter paper separator before and after the discharging test.

	Before Discharging Test	After Discharging Test
C	32.74%	31.47%
O	45.26%	44.63%
K	22.00%	23.90%

Table 4.5: EDX results for glass fiber separator before and after the discharging test.

	Before Discharging Test	After Discharging Test
C	18.37%	12.84%
O	35.21%	38.83%
Al	02.48%	05.55%
Si	15.67%	12.87%
K	28.27%	29.91%
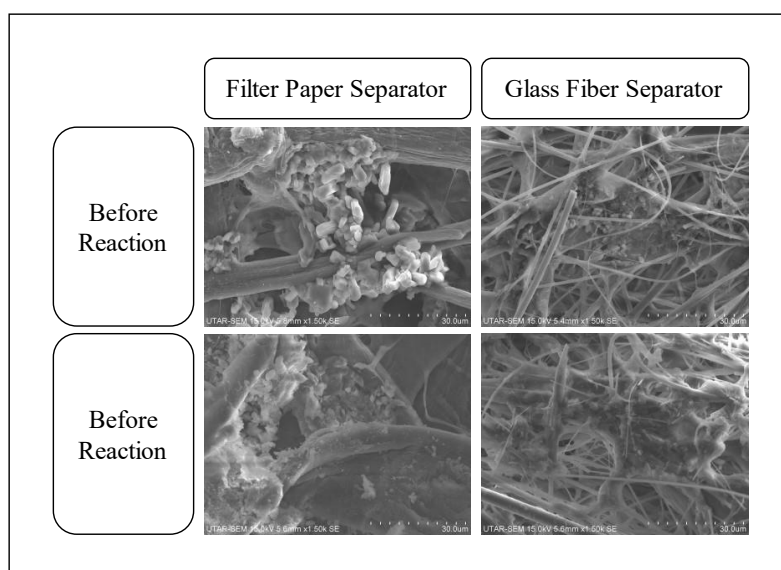
Figure 4.8: SEM results for separators before and after electrochemical reaction under magnification of x1500.

From Figure 4.8, it can be observed that there is formation of precipitates on the surface of the separator after adding ethyl-acetate/KOH electrolyte onto the separator and let the separator dry off before the SEM analysis. After that, from Figure 4.9, it can be observed that there is also formation of precipitates on the surface of the separator. The number of precipitates formed on the surface of the separator does not have drastic changes after the discharging test. In addition, according to Table 4.4 and

Table 4.5, the EDX results also suggest that there are no drastic changes on both separators after the electrochemical reaction since there is only minor element composition changes after the test. These results imply that both separators used in this study has low chemical stability because the precipitate forms even before the discharging test is performed. Again, these experiment results are also similar with the experiment results obtained by Elia, et al. (2017).

4.5   Rechargeable Battery Characterization

The electrically rechargeable AAB in this study was made using aluminium plate as the anode, Cathode 3 (with 400 Mesh and 15 mg rGO loading) as the cathode, glass fiber separator, and ethyl-acetate/KOH as the electrolyte. The battery was connected to the electrochemical workstation to evaluate the charge and discharge performance of the battery. The battery was charged for 10 minutes and then discharged for 10 minutes repeatedly until the discharge potential reached zero. The charge and discharge curve was plotted in the graph shown in Figure 4.9 below.
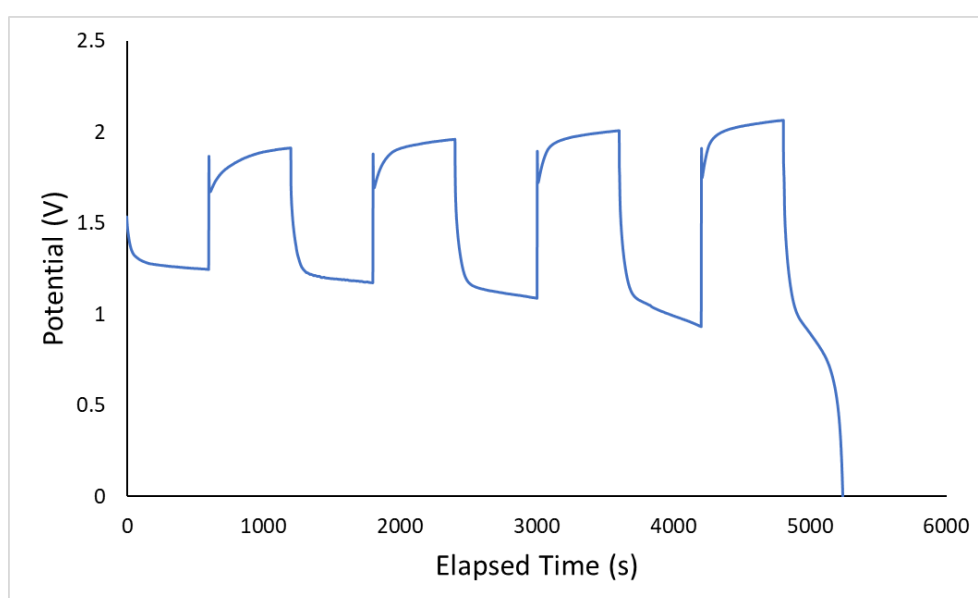

Figure 4.9: Charge and discharge curve.

According to the charge and discharge curve shown in Figure 4.9 above, the curve starts from discharging operation and followed with charging operation. Through observations, it can be observed that the battery discharge

at average potential of 1.25 V at the first discharge cycle. The battery average discharge potential decreases as the charging and discharging cycle increases. As for the charging potential, the average potential of the battery gradually increases as the number of cycle increases. Lastly, it also can be observed that the charge and discharge cycle ended during the discharge operation on the fifth cycle. From this experiment result, the outcome implies that inhibiting the parasitic hydrogen evolution reaction only allows the limited rechargeability of the battery. This experiment result is similar as the experiment results from the Hosseini, et al. (2022).

CHAPTER 5

CONCLUSIONS AND RECOMMENDATIONS

5.1 Conclusions

There are a few of findings that can be concluded from the experiments. First of all, the greater the mesh size of the current collector, the greater the discharge capacity of the battery. Secondly, the optimum loading of reduced graphene oxide is at the mass ratio of 4.5%. Thirdly, using non-woven membrane as battery separator allows better battery performance than cellulose membrane as battery separator. Finally, the experiment shows that the addition of additives into the aqueous electrolyte was able to inhibits the formation for $Al(OH)_3$. However, the suppression of the $Al(OH)_3$ does not provide the battery with long-term rechargeability.

5.2 Recommendations for Future Work

Firstly, according to the articles, the rechargeable AAB can also be developed using ionic liquids containing $AlCl_3$. The feasibility of the ionic liquids containing in contributing to the rechargeability of the AAB in terms of the number of charging and discharging cycles and the changes in the discharging current can be investigated. Other than that, more non-woven membranes that is made using different materials can also be investigated to understand the stability of different materials in the electrolyte.

REFERENCES

Arroyo, F. & Miguel, L. J., 2019. Analysis of Energy Demand Scenarios in Ecuador: National Government Policy Perspectives and Global Trend to Reduce CO2 Emissions. *International Journal of Energy Economics and Policy,* 9(2), pp. 364-374.

Bogolowski, N. & Drillet, J.-F., 2018. Activity of different AlCl3-based electrolytes for the electrically rechargeable aluminium-air battery. *Electrochimica Acta,* Volume 274, pp. 353-358.

Buckingham, R., Asset, T. & Atanassov, P., 2021. Aluminium-air batteries: A review of alloys, electrolytes and design. *Journal of Power Sources,* Volume 498.

Cheng, S. & Wu, J., 2013. Air-cathode preparation with activated carbon as catalyst, PTFE as binder and nickel foam as current collector for microbial fuel cells. *Bioelectrochemistry,* Volume 92, pp. 22-26.

Cho, Y.-J., Park, I.-J., Lee, H.-J. & Kim, J.-G., 2015. Aluminium anode for aluminium–air battery – Part I: Influence of aluminium purity. *Journal of Power Sources,* Volume 277, pp. 370-378.

Day, C. & Day, G., 2017. Climate change, fossil fuel prices and depletion: The rationale for a falling export tax. *Economic Modelling,* Volume 63, pp. 153-160.

Elia, G. A. et al., 2017. Polyacrylonitrile Separator for High-Performance Aluminium Batteries with Improved Interface Stability. *ACS Applied Materials & Interfaces,* Volume 9, pp. 38381-38389.

Gelman, D. et al., 2017. An aluminium - ionic liquid interface sustaining a durable Al-air battery. *Journal of Power Sources,* Volume 364, pp. 110-120.

Goel, P., Dobhal, D. & Sharma, R. C., 2020. Aluminium–air batteries: A viability review. *Journal of Energy Storage,* Volume 28.

Hosseini, S. et al., 2021. The role of SO-group-based additives in improving the rechargeable aluminium-air batteries. *Electrochimica Acta,* Volume 375.

Hosseini, S. et al., 2022. The efficient acetoxy-group-based additives in protecting of anode in the rechargeable aluminium-air batteries. *International Journal of Hydrogen Energy,* Volume 47, pp. 501-516.

Janicek, A., Fan, Y. & Liu, H., 2015. Performance and stability of different cathode base materials for use in microbial fuel cells. *Journal of Power Sources,* Volume 280, pp. 159-165.

Ju, H. et al., 2021. Investigation of pitting corrosion and hydrogen evolution of aluminium and AA2024 alloy by simultaneous electrochemical measurements and imaging. *Electrochemistry Communications,* Volume 132.

Koo, B. et al., 2019. Addition of reduced graphene oxide to an activated-carbon cathode increases electrical power generation of a microbial fuel cell by enhancing cathodic performance. *Electrochimica Acta,* Volume 297, pp. 613-622.

Kuo, Y.-L.et al., 2015. Study of Poly (3,4-ethylenedioxythiophene)/MnO2 as Composite Cathode Materials for Aluminium-Air Battery. *Electrochimica Acta,* Volume 176, pp. 1324-1331.

Li, J. et al., 2018. Cu–MOF-Derived Cu/Cu2O Nanoparticles and CuNxCy Species to Boost Oxygen Reduction Activity of Ketjenblack Carbon in Al–Air Battery. *ACS Sustainable Chemistry & Engineering,* Volume 6, pp. 413-421.

Liu, J. et al., 2012. The effect of water proofing on the performance of nickel foam cathode in microbial fuel cells. *Journal of Power Sources,* Volume 198, pp. 100-104.

Liu, Y. et al., 2017. A comprehensive review on recent progress in aluminium air batteries. *Green Energy and Environment,* Volume 2, pp. 246-277.

Liu, Z. et al., 2021. A reliable gel polymer electrolyte enables stable cycling of rechargeable aluminium batteries in a wide-temperature range. *Journal of Power Sources,* Volume 497.

Li, Y. & Lu, J., 2017. Metal−Air Batteries: Will They Be the Future Electrochemical Energy Storage Device of Choice?. *ACS Energy Letters,* pp. 1370-1377.

Luo, W. et al., 2021. A review of advanced separators for rechargeable batteries. *Journal of Power Sources,* Volume 509.

Luo, Z. et al., 2021. AuPt Nanoparticles/ Multi-Walled carbon nanotubes catalyst as high active and stable oxygen reduction catalyst for Al-Air batteries. *Applied Surface Science,* Volume 564.

Mori, R., 2017a. Electrochemical properties of a rechargeable aluminium–air battery with a metal–organic framework as air cathode material. *The Royal Society of Chemistry,* Volume 7, pp. 6389-6395.

Mori, R., 2017b. Suppression of byproduct accumulation in rechargeable aluminium–air batteries using non-oxide ceramic materials as air cathode materials. *Sustainable Energy & Fuels,* Volume 1, pp. 1082-1089.

Mori, R., 2019. All solid state rechargeable aluminium–air battery with deep eutectic solvent based electrolyte and suppression of byproducts formation. *RSC Adv,* Volume 9, pp. 22220-22226.

Mori, R., 2020. Recent Developments for Aluminium–Air Batteries. *Electrochemical Energy Reviews,* pp. 344-369.

Nguyen, T. H., Fraiwan, A. & Choi, S., 2014. Paper-based batteries: A review. *Biosensor and Bioelectronics,* Volume 54, pp. 640-649.

Park, I.-J., Choi, S.-R. & Kim, J.-G., 2017. Aluminium anode for aluminium-air battery - Part II: Influence of In addition on the electrochemical characteristics of Al-Zn alloy in alkaline solution. *Journal of Power Sources,* Volume 357, pp. 47-55.

Qin, Y. et al., 2020. Advanced Filter Membrane Separator for Aqueous Zinc-Ion Batteries. *Small,* 16(39).

Revel, R., Audichon, T. & Gonzalez, S., 2014. Non-aqueous aluminium-air battery based on ionic liquid electrolyte. *Journal of Power Sources,* Volume 272, pp. 415-421.

Sengupta, I. et al., 2018. Thermal reduction of graphene oxide: How temperature influences purity. *Journal of Materials Research,* Volume 33, pp. 4113-4122.

Sengupta, I., Kumar, S. S. S., Pal, S. K. & Chakraborty, S., 2020. Characterization of structural transformation of graphene oxide to reduced graphene oxide during thermal annealing. *Journal of Materials Research,* Volume 35, pp. 1197-1204.

Sun, S. et al., 2016. Oxygen reduction reaction catalysts of manganese oxide decorated by silver nanoparticles for aluminium-air batteries. *Electrochimica Acta,* Volume 21, pp. 49-55.

Tang, Y. et al., 2018. Advanced batteries based on manganese dioxide and its composites. *Energy Storage Materials,* Volume 12, pp. 284-309.

Tan, W. C. et al., 2021. Analysis of the Polypropylene-Based Aluminium-Air Battery. *Frontiers in Energy Research,* Volume 9.

Vazhayil, A. et al., 2021. A comprehensive review on the recent developments in transition metal-based electrocatalysts for oxygen evolution reaction. *Applied Surface Science Advances,* Volume 6.

Woodford, C., 2021. *Batteries.* [Online] Available at: https://www.explainthatstuff.com/batteries.html [Accessed 10 February 2022].

Wu, F. et al., 2018. An interface-reconstruction effect for rechargeable aluminium battery in ionic liquid electrolyte to enhance cycling performances. *Green Energy & Environment,* Volume 3, pp. 71-77.

Xia, Z. et al., 2020. Cobalt ion intercalated MnO2/C as air cathode catalyst for rechargeable aluminium-air battery. *Journal of Alloys and Compounds,* Volume 824.

Zhang, S. S., 2007. A review on the separators of liquid electrolyte Li-ion batteries. *Journal of Power Sources,* Volume 164, pp. 351-364.

Zhang, X. et al., 2015. N-type Cu2O doped activated carbon as catalyst for improving power generation of air cathode microbial fuel cells. *Bioresource Technology,* Volume 187, pp. 299-304.

Zhuang, Z.-h.et al., 2021. Effect of Ga on microstructure and electrochemical performance of Al–0.4Mg–0.05Sn–0.03Hg alloy as anode for Al–air batteries. *Transactions of Nonferrous Metals Society of China,* Volume 31, pp. 2558-2569.